HHS Public Access

Author manuscript

*Nature*. Author manuscript; available in PMC 2024 August 19.

Published in final edited form as:

*Nature*. 2023 December ; 624(7990): 207–214. doi:10.1038/s41586-023-06761-7.

# TMPRSS2 is a functional receptor for human coronavirus HKU1

**Nell Saunders**[1], **Ignacio Fernandez**[2], **Cyril Planchais**[3], **Vincent Michel**[4], **Maaran Michael Rajah**[1], **Eduard Baquero Salazar**[5], **Jeanne Postal**[1], **Francoise Porrot**[1], **Florence Guivel-Benhassine**[1], **Catherine Blanc**[6], **Gaëlle Chauveau-Le Friec**[7], **Augustin Martin**[1], **Ludivine Grzelak**[1], **Rischa Maya Oktavia**[2], **Annalisa Meola**[2], **Olivia Ahouzi**[2], **Hunter Hoover-Watson**[1], **Matthieu Prot**[8], **Deborah Delaune**[8,13], **Marion Cornelissen**[9,10], **Martin Deijs**[10,11], **Véronique Meriaux**[7], **Hugo Mouquet**[3], **Etienne Simon-Lorière**[8,14], **Lia van der Hoek**[10,11], **Pierre Lafaye**[7], **Felix Rey**[2], **Julian Buchrieser**[1,#,*], **Olivier Schwartz**[1,12,#,*]

[1]Virus & Immunity Unit, Institut Pasteur, Université de Paris Cité, CNRS UMR 3569, Paris, France

[2]Structural Virology Unit, Institut Pasteur, Université de Paris Cité, CNRS UMR 3569, Paris, France

[3]Humoral Immunology Unit, Institut Pasteur, Université de Paris Cité, INSERM U1222, Paris, France

[4]Pathogenesis of Vascular Infections Unit, Institut Pasteur, INSERM, Paris, France.

[5]Nanoimaging core, Institut Pasteur, Université de Paris Cité, INSERM U1222, Paris, France

[6]Pasteur-TheraVectys Joint Lab, Institut Pasteur, Université de Paris Cité, Paris, France

[7]Antibody Engineering Platform, C2RT, Institut Pasteur, Université de Paris Cité, CNRS UMR 3528, Paris, France.

[8]G5 Evolutionary Genomics of RNA Viruses, Institut Pasteur, Paris, France.

[9]Department of Medical Microbiology and Infection Prevention, Amsterdam UMC, Molecular Diagnostic Unit, University of Amsterdam, 1105 AZ Amsterdam, Netherlands.

[10]Amsterdam Institute for Infection and Immunity, Amsterdam, The Netherlands

[11]Department of Medical Microbiology and Infection Prevention, Amsterdam UMC, Laboratory of Experimental Virology, University of Amsterdam, 1105 AZ Amsterdam, Netherlands.

[12]Vaccine Research Institute, Creteil, France

---



[*]Correspondence and requests for materials should be addressed to Olivier Schwartz.

[#]Co-last authors

Author contributions

Experimental strategy design: NS, IF, CP, MMR, HM, FR, JB, OS

Data acquisition and analysis: NS, IF, CP, VM, MMR, EBS, FP, FGB, JP, CB, AMa, LG, MOR, AMe, OA, HHW, MP, DD, ESL, JB

Vital materials and expertise: GCLF, MC, MD, VM, LVDH, PL

Manuscript writing: NS, JB, OS

Manuscript editing: NS, IF, CP, EBS, HM, FR, PL, JB, OS

All authors read and approved the final version of the manuscript.

Supplementary Information is available for this paper.

Conflict of interest

NS, JB, OS, IF, EB, FAR, and PL have a provisional patent on anti-TMPRSS2 nanobodies.

[13]Institut de Recherche Biomédicale des Armées, Brétigny-sur-Orge, France

[14]National Reference Center for viruses of respiratory infections, Institut Pasteur, Paris, France.

## Abstract

Four endemic seasonal human coronaviruses causing common colds, HKU1, 229E, NL63 and OC43 circulate worldwide[1]. After binding to cellular receptors, coronavirus spike proteins are primed for fusion by transmembrane-serine protease 2 (TMPRSS2) or endosomal cathepsins[2–9]. NL63 uses angiotensin-converting enzyme 2 (ACE2) as a receptor[10], whereas 229E uses human aminopeptidase-N[11]. HKU1 and OC43 spikes bind cells through 9-O-acelytated sialic acid but their protein receptors remain unknown[12]. Here, we show that TMPRSS2 is a functional receptor for HKU1. TMPRSS2 triggers HKU1 spike-mediated cell-cell fusion and pseudovirus infection. Catalytically inactive TMPRSS2 mutants do not cleave HKU1 spike but allow pseudovirus infection. Furthermore, TMPRSS2 binds with high affinity to the HKU1 receptor binding domain (RBD) ($K_d$ 334 and 137 nM for HKU1A and HKU1B genotypes) but not to SARS-CoV-2. Conserved amino acids within HKU1 RBD are essential for binding to TMPRSS2 and pseudovirus infection. Newly designed anti-TMPRSS2 nanobodies potently inhibit HKU1 spike attachment to TMPRSS2, fusion and pseudovirus infection. The nanobodies also reduce infection of primary human bronchial cells by an authentic HKU-1 virus. Our findings illustrate the various evolution strategies of coronaviruses, which use TMPRSS2 to either directly bind to target cells or to prime their spike for membrane fusion and entry.

HKU1 was first identified from an elderly patient with severe pneumonia in Hong Kong in 2005[13]. HKU1 was later shown to cause common cold and benign respiratory symptoms, but complications include severe lower respiratory infections, particularly in young children, the elderly and immunocompromised individuals[14]. It is estimated that 70% of children seroconvert before the age of 6[15]. The global seroprevalence of HKU1 is similar to other seasonal human coronaviruses (hCoV) and is between 75 and 95%[15–17]. Three main viral genotypes have been identified, HKU1A, B and C. HKU1A and B spikes have 85% identity (Fig. 1a). HKU1C is a HKU1A/B recombinant and its spike shares 99% identity with HKU1B. Conserved regions in the HKU1A and B spikes include a putative RBD with a Receptor Binding Motif (RBM)[18,19], S1/S2 and S2/S2’ cleavage sites[20] (Fig.1a).

Both HKU1 and OC43 spikes bind to 9-O-acetylated α2,8 linked disialosides on target cells[12,21,22]. Their protein receptors have not been identified. After receptor binding, the coronavirus spike is cleaved at the S2’ site by membrane bound proteases, such as TMPRSS2, or by endosomal cathepsins, resulting in a conformational change of S2 that projects the fusion peptide into the target membrane to drive fusion[23]. TMPRSS2 belongs to the type II transmembrane serine protease (TTSP) family that comprises 19 cell-surface enzymes[24,25]. TTSPs are involved in many processes, including epithelial homeostasis, extracellular matrix degradation, hormone and growth factor activation, and initiation of proteolytic cascades through cleavage of membrane cellular proteins[24]. TMPRSS2 primes coronavirus spikes and other viral envelope glycoproteins, such as influenza hemagglutinin, enabling fusion[26]. TTSPs are synthesized as single-chain proenzymes that require proteolytic activation[24]. TMPRSS2 undergoes autocleavage into two subunits that

remain attached by a disulfide bond[27]. In the respiratory tract, TMPRSS2 is expressed in nasal, bronchial and small airways tissues, and more particularly in ciliated cells that are the main target of HKU1[28,29]. Here, using cell-cell fusion assays, infections with pseudovirus and live virus, as well as *in vitro* binding tests, we identify TMPRSS2 as a high-affinity receptor for HKU1.

## Generation of anti-TMPRSS2 nanobodies

To our knowledge, there are no currently available anti-TMPRSS2 antibodies that allow cell surface staining, as most of the existing ones are directed towards cytosolic fragments of the protein. We thus immunized an alpaca with the soluble ectodomain of a catalytically inactive TMPRSS2 (S441A mutant) to produce VHH single-chain nanobodies. We isolated 5 VHHs (A01, F05, A07, C11 and D01) that bind with an affinity in the nanomolar range to soluble S441A TMPRSS2 (Extended Data Fig. 1a, Extended Data Table 1). We selected one VHH with the highest affinity (A01) in order to generate a dimeric antibody with a human Fc domain that efficiently stained TMPRSS2+ cells (Extended Data Fig. 1b).

## TMPRSS2 triggers spike-dependent fusion

To investigate the effect of TMPRSS2 on HKU1 spike mediated fusion, we generated plasmids encoding for the HKU1A (isolate N1 - NCBI: txid443239) and B (Isolate N5 - NCBI: txid443241) spikes (Fig. 1a). In 293T cells that do not express TMPRSS2, transient transfection led to surface expression of the two proteins, as assessed by flow cytometry using mAb10, a pan S2 coronavirus antibody[30] (Extended Data Fig. 2a). To study cell-cell fusion, we used a GFP-Split based model in which fused cells become GFP+ (Fig. 1b)[31]. HKU1A and B spikes did not induce fusion alone but were highly fusogenic when co-expressed with TMPRSS2 in 293T cells (Fig. 1b, Extended Data Fig. 2b). In contrast, in experiments run in parallel, the SARS-CoV-2 spike induced fusion when co-expressed with ACE2 and not with TMPRSS2 (Extended Data Fig. 2c). HKU1 also triggered syncytia when co-expressed with TMPRSS2 in U2OS cells (Extended Data Fig. 2d).

As a control of specificity for HKU1 fusion, we tested a panel of 12 other surface proteases, including the coronavirus receptors aminopeptidase-N (APN), dipeptidyl peptidase-4 (DPP4) and ACE2, as well as TMPRSS4 and TMPRSS11D, that have been reported to cleave the SARS-CoV-2 spikes[32–34]. The proteases were correctly expressed, as assessed by flow cytometry (Extended Data Fig. 2e-i), but only TMPRSS2 triggered cell-cell fusion (Fig. 1c).

We next generated fluorescent TMPRSS2-mNeonGreen and HKU1A Spike-mScarlet-I to follow fusion by video microscopy. When mixed 24 h after transfection, cells expressing spike and cells expressing TMPRSS2 formed syncytia in less than 1 h, indicating that this process is rapid (Extended Data Fig. 2j, Supp. videos 1-2). By expressing TMPRSS2 either on donor cells (spike-transfected) or acceptor cells, we observed that the protease had to be on acceptor cells, opposite of the spike to induce high levels of fusion (Fig. 1d).

We then investigated whether endogenous levels of TMPRSS2 were sufficient to induce HKU1 spike-dependent fusion. We mixed HKU1A spike-expressing 293T donor cells with

Caco2 acceptor cells, that endogenously express low levels of TMRPSS2[35] (Extended Data Fig. 3). Spike expressing cells fused with parental Caco2 cells but not with Caco2 TMPRSS2-KO cells, a Caco2 derivative in which the *tmprss2* gene was knocked down by CRISPR-Cas9 (Fig. 1e, Extended Data Fig. 3a-c). Silencing of TMPRSS2 using siRNA in Caco2 cells also significantly reduced fusion with spike-expressing 293T cells (Extended Data Fig. 3d).

Altogether, these results indicate that TMPRSS2 expression enables HKU1A and B spike-mediated cell-cell fusion.

## Inactive TMPRSS2 allows HKU1 infection

To further analyze the role of TMPRSS2 in HKU1 spike fusion, we generated two well-characterized TMPRSS2 mutants, R255Q and S441A[27] (Fig. 2a). R255 is in the auto-cleavage site, and S441 is in the catalytic site; both mutations prevent TMPRSS2 autocleavage and activity. As expected, R255Q and S441A were correctly expressed in 293T cells but lacked catalytic activity, measured with a substrate generating a fluorescent signal upon cleavage[36] (Extended Data Fig. 4a). We then studied the cleavage profile of TMPRSS2 and HKU1 spike by western blot (Fig. 2b). We focused our analysis on HKU1A spike since none of the polyclonal or monoclonal antibodies tested recognized the HKU1B spike by western blot. When expressed alone, WT TMPRSS2 was cleaved while the mutants were not. When the HKU1 spike was present, a similar profile of TMPRSS2 processing was observed. Without TMPRSS2, the spike was partially cleaved into S1 and S2 subunits (Fig. 2b), most likely at the polybasic furin cleavage S1/S2 site (Fig. 1a). WT TMPRSS2, but not the catalytically inactive R255Q and S441A mutants, generated additional cleavage bands in the spike, including a 100 kDa band below the S2 band, which likely corresponds to the S2' fragment.

We then examined how the spike was cleaved by TMPRSS2 present on adjacent cells. To this aim, we mixed spike expressing cells with TMPRSS2 expressing cells. We assessed by western blot the processing of the spike 3 and 6 h after coculture (Extended Data Fig. 4b). The spike cleavage by WT TMPRSS2 was slightly visible 3 h after coculture, and this process was more marked at 6 h. Of note, syncytia were detected at 3 and 6 h post co-culture in the WT TMPRSS2 condition.

The WT and mutant TMPRSS2 had slightly different levels of expression upon transfection in 293T cells, when assessed by flow cytometry (Extended Data Fig. 4c, d). We thus adjusted the amounts of plasmids to reach similar levels. The catalytically inactive TMPRSS2 mutants barely induced cell-cell fusion with either HKU1A or B spikes (Fig. 2c), confirming the need of spike cleavage for cell-cell fusion.

We next generated single-cycle HKU1 pseudoviruses − lentiviral particles pseudotyped with HKU1 spikes − to further investigate the role of TMPRSS2 in HKU1 entry. The pseudovirus strategy has been successfully used to study SARS-CoV-2 entry and to identify ACE2 as a receptor for this virus[37]. HKU1A and B pseudoviruses did not infect parental 293T cells efficiently, while transient expression of TMPRSS2 enabled high viral entry (Fig. 2d).

In striking contrast with their inability to trigger cell-cell fusion, the catalytically inactive R255Q and S441A TMPRSS2 mutants readily allowed infection of 293T cells with HKU1A or HKU1B pseudovirus (Fig. 2d). The TMPRSS2 mutants behave as expected regarding the SARS-CoV-2 spike (D614G ancestral strain), which requires the enzymatic activity of the protease for infectivity enhancement[37]. In 293T-ACE2 cells, WT TMPRSS2 increased SARS-CoV-2 pseudotype entry by 8-fold, whereas this was not the case for the R255Q and S441A mutants (Extended Data Fig. 4e). Together, our data show that catalytic activity of TMPRSS2 is not required for HKU1-mediated pseudovirus entry.

Coronavirus spike can either be processed by proteases at the surface of target cells, allowing for membrane fusion, or by cathepsins in endosomes, allowing for entry after internalization[8]. As TMPRSS2 catalytic activity was not required for HKU1 entry, we examined the cytoplasmic access route of pseudovirus in 293T cells expressing WT or S441A TMPRSS2. To this aim, we performed infections in presence of SB412515, a cathepsin L inhibitor, or E64d, a pan-cysteine protease inhibitor. The drugs were added 2 h before infection and maintained for 48 h. SB412515 and E64d reduced the entry of HKU1A pseudovirus in S441A TMPRSS2 cells and not in WT TMPRSS2 cells (Extended Data Fig. 4f). This strongly suggests that viral entry occurs through endosomes with the catalytically inactive TMPRSS2 and at the surface with the WT protease. With HKU1B, SB412515 and E64d had little or no effect on entry (Extended Data Fig. 4g), suggesting that HKU1B might be cleaved by other proteases or requires less cleavage to induce fusion, although it still uses TMPRSS2 as a receptor. Infection by both HKU1A and HKU1B pseudoviruses was inhibited by hydroxychloroquine (HCQ) in S441A TMPRSS2 cells, confirming an endocytic route with the mutant protease (Extended Data Fig. 4f, g).

We next asked whether TMPRSS2 could confer sensitivity to HKU1 pseudovirus in other cell lines. We generated U2OS and A549 stably expressing WT or S441A TMPRSS2. We reintroduced the two proteins in Caco2 TMPRSS2-KO cells. Flow cytometry demonstrated that TMPRSS2 was expressed in this panel of cells (Extended Data Fig. 4h, i). The presence of WT or S441A TMPRSS2 enabled infection to various extents of U2OS, A549 and Caco2 cells by HKU1A and HKU1B pseudoviruses (Fig. 2e). Knock-out of TMPRSS2 significantly reduced entry into Caco2 cells. Furthermore, in parental Caco2 cells, preincubation with Camostat, a serine protease inhibitor known to inhibit TMPRSS2, did not affect HKU1 pseudovirus infection, while, as expected, it diminished SARS-CoV-2 entry by two-fold (Extended Data Fig 4j), confirming the role of endogenous TMPRSS2 as a receptor.

The Vero E6-TMPRSS2 cell line[38] remained insensitive to HKU1 pseudovirus infection (Extended Data Fig. 4k). Vero E6 cells are African green monkey kidney cells, it is thus possible that other parameters (glycosylation, sialylation, adhesion molecules or other cellular proteins, etc…) may regulate their sensitivity to HKU1.

We then analyzed the role of sialic acids during TMPRSS2-mediated HKU1 entry. We treated U2OS TMPRSS2+ cells with Neuraminidase, an enzyme that removes (α2,3), (α2,6) and (α2,8) linked sialic acids. Neuraminidase decreased binding of two sialic acid ligands, Lectin SNA and Siglec E, without affecting surface levels of TMPRSS2 (Extended data Fig.

5). Neuraminidase reduced sensitivity of target cells to HKU1 pseudovirus infection in a dose-dependent manner, suggesting that sialic acids are necessary to trigger efficient HKU1 entry in TMPRSS2+ cells (Extended data Fig. 5).

Taken together, our results show that TMPRSS2 is required for HKU1 pseudovirus infection but that its catalytic activity is dispensable, possibly because it can be rescued by other proteases such as cathepsins.

## HKU1 spike binds to TMPRSS2

We next generated recombinant ectodomains of HKU1A and B spikes to investigate their binding to TMPRSS2 expressing cells (Fig. 3a, b, Extended Data Fig. 6a). HKU1 spike bound weakly to WT TMPRSS2 and more strongly to TMPRSS2 S441A and R255Q, as assessed by flow cytometry. Addition of Camostat increased binding to WT TMPRSS2 (Fig. 3b, Extended Data Fig. 6a), indicating that the proteolytic activity of TMPRSS2 somehow interfered with our readout or decreased binding by degrading or shedding the bound spike. Alternatively, WT TMPRSS2's turnover might be faster than the mutants'. As expected, with a soluble SARS-CoV-2 spike, we detected binding to cells expressing ACE2 but not WT or mutant TMPRSS2 (Fig. 3b, Extended Data Fig. 6a, b), highlighting the different behaviors of HKU1 and SARS-CoV-2.

We then showed binding of the recombinant TMPRSS2 ectodomain to the HKU1A or B spikes by ELISA, but not to the SARS-CoV-2 spike (Fig. 3c). This indicates a direct interaction between TMPRSS2 and the HKU1 spike. Conversely, soluble ACE2 bound the SARS-CoV-2 but not the HKU1 spike by ELISA (Extended Data Fig. 6c). Due to the low yield of soluble WT TMPRSS2, we generated a soluble S441A mutant that could be obtained in amounts that allowed biophysical experiments. We expressed RBDs of the different viruses (residues 323–609 for HKU1A; 323–607 for HKU1B; 331–528 for SARS-CoV-2) to measure their affinity for S441A TMPRSS2 by biolayer interferometry (BLI). The RBDs from HKU1A and B interacted strongly with TMPRSS2, while the interaction of the SARS-CoV-2 RBD with TMPRSS2 was comparable to that of an irrelevant control protein (CD147) (Fig. 3d and Extended Data Fig. 6d-e). Using a range of S441A TMPRSS2 concentrations, affinity constants ($K_d$) of 334 nM and 137 nM were determined for HKU1A and B RBDs, respectively (Table 1, Extended Data Fig. 6d-e, SI 5, 6). The SARS-CoV-2 RBD bound to the ectodomain of ACE2 with a $K_d$ of 92 nM (Extended Data Fig. 6f, Table 1).

## HKU1 spike receptor binding motif

The residues W515 and R517 within the HKU1 RBD[19] have been reported to be critical for binding to an unknown cellular receptor[18]. We produced the recombinant HKU1B RBD with the W515A or R517A mutations. As assessed by BLI, the W515A mutation abrogated interaction with TMPRSS2, reaching response levels comparable to those obtained with a control protein, while the R517A mutation reduced binding by 2.8-fold ($K_d$=376 nM) (Fig. 3e, Extended Data Fig. 6g, h, Table 1, SI 5, 6). We also generated plasmids coding for the HKU1A and HKU1B spikes with the W515A or R517A mutations. These mutants were

correctly expressed at the cell surface, as assessed by flow cytometry (Extended Data Fig. 6i) but they lost their cell-cell fusion properties in the presence of TMPRSS2 (Fig. 3f). Their ability to trigger pseudovirus entry was decreased by 2 to 3 logs, resulting in infection levels close to background (Fig. 3g). Therefore, the conserved W515 and R517 residues within the HKU1A and B RBDs are critical for binding to TMPRSS2, viral fusion and entry.

## Anti-TMPRSS2 VHHs block spike binding

We then examined whether the anti-TMPRSS2 VHH inhibited the HKU1 receptor function or the enzymatic activity of the protease. The 5 VHHs (A01, F05, A07, C11 and D01) efficiently bound soluble S441A TMPRSS2 as assessed by BLI (Extended Data Fig. 1a and Extended Data Table 1) and flow cytometry (Extended Data Fig. 7a). Three VHH (A07, C11 and D01) inhibited the HKU1B RBD–interaction with S441A TMPRSS2 measured by BLI (Fig. 4a). The same three VHH reduced TMPRSS2 catalytic activity (Extended Data Fig. 7b). Those nanobodies also inhibited HKU1A and B spike – TMPRSS2 mediated cell-cell fusion (Fig. 4b, Extended Data Fig. 7c). We then examined their effect on viral entry independently of their inhibition of the catalytic activity of TMPRSS2. They reduced pseudovirus infection of 293T cells expressing S441A TMPRSS2 in a dose-dependent manner (Fig. 4c, Extended Data Fig. 7d). The two other nanobodies (A01 and F05), despite showing efficient binding to TMPRSS2, did not interfere with its enzymatic activity and proviral roles (Fig. 4b, c and Extended Data Fig. 7c-d), suggesting that they bind to regions different from those of three active VHHs and that are not involved in HKU1 spike binding.

## Anti-TMPRSS2 VHH blocks HKU1 infection

HKU1 does not grow in any cell line tested up to date but viral amplification in human ciliated airway epithelial cell cultures has been reported[29,39,40]. We isolated an HKU1 virus from a nasal swab of an individual suffering from a respiratory tract infection. To this end, we used primary human bronchial epithelial cells (HBE cells) differentiated at the air/liquid interface (ALI) for over 4 weeks. We first examined whether these cells were positive for TMPRSS2. Immunofluorescence of HBE cells with the anti-TMPRSS2 VHH-A01-Fc revealed a preferential staining of ciliated cells, with a positive signal accumulating at the cilia (Fig. 5a). We then amplified the virus from the clinical sample by one passage on HBE cells. We observed an increase of HKU1 viral RNA in apical culture supernatants, with concentrations peaking at $5\times10^6$ viral RNA copies/μL at 2–3 days post-infection (dpi) (Extended Data Fig. 8a). Metagenomic sequencing of the viral supernatant identified a HKU1 genotype B (Extended Data Fig. 8b), and no other virus was detected. For reasons that remain to be elucidated, our attempts to further grow this HKU1B isolate in various cell lines, expressing WT or S441 TMPRSS2 were unsuccessful. However, the virus grew on a second passage on HBE cells, indicating that it was infectious (Extended Data Fig. 8a).

We then asked whether the anti-TMPRSS2 nanobodies inhibited infection of HBE cells. We preincubated target cells with the A07 VHH or a control nanobody and measured the spike intensity by immunofluorescence 48 h post-infection (Fig. 5b). The A07 VHH strongly reduced the appearance of infected cells, indicating that the spike binding and/or cleavage activities of TMPRSS2 are necessary for a productive HKU1 infection.

## Discussion

Here, we demonstrate that TMPRSS2 is a receptor for HKU1. TMPRSS2 triggers HKU1-mediated cell-cell fusion, viral entry and binds with high affinity to both HKU1A and HKU1B RBDs. The enzymatic activity of TMPRSS2 is required for HKU1-dependent cell-cell fusion but not for entry of HKU1 pseudovirus. Two cathepsin inhibitors decrease HKU1A pseudovirus infection mediated by the catalytically inactive TMPRSS2, but not by the wild-type protease. This strongly suggests that after viral binding to TMPRSS2, viral particles expressing HKU1A can either fuse at the plasma membrane if the protease is active or be internalized and processed in the endosomal compartment when the protease is inactive. For HKU1B, other mechanisms could be at play.

TMPRSS2 directly binds to HKU1 but not to SARS-CoV-2 spikes. The autocleavage of TMPRSS2 is not required for binding. The affinity of HKU1A and HKU1B ($K_d$ = 334 and 131 nM, respectively) is slightly below what we measured for the SARS-CoV-2 RBD interaction with ACE2 ($K_d$ = 92 nM). A conserved groove in a region of HKU1A and B spikes composed of amino acid 505, 515, 517–521 and 528 has been proposed to be involved in binding to an unknown receptor[18,19]. We show that the 515 and 517 residues of the spike are essential for efficient binding to TMPRSS2, viral fusion and entry, thus adding evidence that this region may be part of the RBM. Further structural studies are warranted to precisely map the amino-acids and regions allowing the interactions between the spike and its receptor. Another protease, Kalikrein 13 (KLK13) has been reported to cleave HKU1 spike[41]. Future work will help addressing how KLK13 may modulate HKU1 interaction with TMPRSS2.

We further designed anti-TMPRSS2 VHH that inhibit TMPRSS2 binding to HKU1 spikes and prevent cell-cell fusion and viral entry. The anti-TMPRSS2 nanobodies inhibit the enzymatic activity of TMPRSS2 and hinder HKU1 pseudovirus entry using S441A TMPRSS2. This strongly suggests that the spike binds close to the catalytic site of the enzyme. These nanobodies confirmed the role of TMPRSS2 as a HKU1 receptor and provide useful tools to interfere with TMPRSS2 function. TMPRSS2 also plays a role in the development of certain cancers[42]. It will be worth studying how these nanobodies may target tumor cells or inhibit infection of viruses relying on this enzyme, as an alternative to small molecule inhibitors[43].

Finally, we isolated an HKU1B live virus and report that TMPRSS2 is required for productive infection of primary HBE cells, that are natural targets of the virus. It will be of interest to further determine whether the HKU1 binding property, the enzymatic activity or most likely both functions of TMPRSS2 are necessary to trigger HKU1 infection in these primary cells. We were so far unable to amplify the virus in cell lines. Future work will be necessary to understand which step of the viral life cycle is impaired in TMPRSS2+ cell lines, or if another factor is required. It will be also worth examining whether soluble TMPRSS2, known to be shed in the extracellular space, may interfere with HKU1 entry.

Human coronavirus receptors that have been identified so far and allow productive viral entry are cell surface proteases. TMPRSS2 and other TTSP are known to prime human

coronaviruses for fusion by cleaving their spikes, generally after viral binding to target cells. Of note, Omicron strains rely less on TMPRSS2 than previous SARS-CoV-2 lineages, reflecting a constant adaptation of coronaviruses to their hosts[44]. Our study provides the first evidence that TMPRSS2 also acts as a direct physical receptor for HKU1 entry, in addition to its previously known role in cleaving the spike. ACE2 binding is an ancestral and evolvable trait of sarbecoviruses[45,46] . TMPRSS2 binding may represent another parameter of coronavirus evolution. Whether coronaviruses have lost affinity or sensitivity to TMPRSS2 during evolution, or whether HKU1 has gained affinity for human or animal TMPRSS2 remains to be determined. Our results highlight the critical role of TMPRSS2 and other proteases as determinants of coronavirus tropism and pathogenesis[23].

## Methods

### Plasmids

Codon-optimized HKU1A (RefSeq: YP_173238.1) and B/C isolate N5P8, referred to HKU1B (UniProtKB/Swiss-Prot: Q0ZME7.1) full spikes were ordered as synthetic genes (GeneArt, Thermo Fisher Scientific) and cloned into a phCMV backbone (GeneBank: AJ318514), by replacing the VSV-G gene. pQCXIP-Empty control plasmid was previously described[31]. pQCXIP-BSR-GFP11 and pQCXIP-GFP1–10 were a kind gift from Yutaka Hata[47] (Addgene plasmid #68716 and #68715). pCSDest-TMPRSS2 was a kind gift from Roger Reeves[48] (Addgene plasmid # 53887). Mutations in the HKU1 spike and TMPRSS2 were introduced using the NEB Q5 Side-Directed mutagenesis kit. Plasmids were sequenced before usage. phCMV-HKU1-S-mNeonGreen and pCDEST-TMPRSS2-mScarlet-I were generated by Gibson assembly. pCAGGS-based expression vectors N-terminal cMYC-epitope tagged TMPRSS2, TMPRSS3, TMPRSS4, TMPRSS10, TMPRSS11A, TMPRSS11B, TMPRSS11D, TMPRSS11E, TMPRSS11F and TMPRSS13 were a kind gift from Stefan Pöhlmann[34]. pLV-EF1a-IRES-Hygro was a gift from Tobias Meyer (Addgene plasmid # 85134)[49]. pLV-EF1a-DEST-IRES-Hygro was generated by Gibson assembly. pLV-TMPRSS2-Hygro was generated by cloning TMPRSS2 from pCSDest-TMPRSS2 into pLV-EF1a-DEST-IRES-Hygro using gateway cloning. pLV-TMPRSS2-S441A-Hygro and pLV-TMPRSS2-R255Q-Hygro were generated by Q5 site directed mutagenesis (New England Biolabs).

### Cells

HEK293T (293T), U2OS, VeroE6, A549 and Caco2/TC7 (Caco2) were from ATCC and cultured in DMEM with 10% fetal bovine serum (FBS) and 1% penicillin/streptomycin (PS). GFP-split cells were previously described[31] and cultured with 1 μg/mL of puromycin (InvivoGen). Cells stably expressing TMPRSS2 were cultured with 100 μg/mL hygromycin. Cells were routinely screened for mycoplasma. Cells were authenticated by genotyping (Eurofins).

### Reagents

SB412515 was purchased from Cayman Chemical, E64d and Camostat mesylate from Sigma Aldrich, hydroxychloroquine from Merck, Neuraminidase (or Sialidase from *Arthrobacter ureafaciens)* from Roche.

### Sequence alignments

Alignments of HKU1 A and B spikes in Fig. 1a were performed using Protein Blast with default settings (NCBI). Alignment figures were generated using the seqvisr package in R (GitHub: 10.5281/zenodo.6583981).

### GFP-split fusion assay

Cell–cell fusion assays were performed as previously described[31,50]. Briefly, 293T cells stably expressing GFP1–10 and GFP11 were co-cultured at a 1:1 ratio ($6 \times 10^4$ cells/well) and transfected in suspension with Lipofectamine 2000 (Thermo) in a 96-well plate (uClear, #655090) (10 ng of spike plasmid, indicated amounts of TMPRSS2 plasmids adjusted to 100 ng DNA with pQCXIP-Empty). For Acceptor-Donor experiments, 293T GFP-split cells (GFP1-10 and GFP11) were transfected separately in suspension with 500 ng of DNA (10% spike, indicated amounts of TMPRSS2 plasmid adjusted to 500 ng with pQCXIP-Empty) for 30 min at 37°C. Cells were washed twice and acceptor and donor cells were mixed and seeded at $6 \times 10^4$ cells/well. For Caco2 KD experiments, Caco2 GFP11 cells were transfected with control siRNA-directed against Luciferase: 5′-CGUACGCGGAAUACUUCGA-3′ or siGENOME Human TMPRSS2 SMARTpool (#7113 - Horizon Discovery) at 50 nM using Lipofectamine™ RNAiMAX (Thermo Fisher Scientific) in a 6 well dish for 48 h. 293T GFP1–10 cells were transfected with 10% of spike plasmid in a 6 well dish for 24 h. Caco2 KD or Caco2 KO cells and 293T spike cells were mixed at a 1:1.5 ratio in a 96 well plate. The remaining Caco2 cells were used for RNA extraction for qPCR. For all experiments, at 20 h post-transfection, images covering 90% of the well surface, were acquired per well on an Opera Phenix High-Content Screening System (PerkinElmer). The GFP area was quantified on Harmony High-Content Imaging and Analysis Software.

### RNA Extraction, Reverse Transcription, and qPCR

At 48 h post siRNA transfection, $5 \times 10^5$ Caco2 cells were lysed using RLT buffer (QIAGEN) supplemented with 10 µL of β-mercaptoethanol. RNA extraction was performed using the RNeasy plus mini kit (QIAGEN) according to the manufacturer's protocol. Reverse transcription was performed using SuperScript II (Thermo Fisher Scientific) according to the manufacturer's protocol. qPCR was performed using iTaq universal SYBR green supermix (Bio Rad) on a QuantStudio 6 Real-Time PCR machine (Thermo Fisher Scientific). The following primers were used: β-Tubulin forward: 5'-CTTCGGCCAGATCTTCAGAC-3', reverse: 5'-AGAGAGTGGGTCAGCTGGAA-3'; TMPRSS2 forward: 5'-GGGGATACAAGCTGGGGTTC-3', reverse: 5'-GATTAGCCGTCTGCCCTCAT-3'.

### HKU1-spike-TMPRSS2 video microscopy

One million 293T cells were transfected either with 1 µg of pCDEST-TMPRSS2-scarlet-I or phCMV-HKU1A S-NeonGreen plasmid in a 6-well plate using lipofectamine 2000 according to the manufacturer's protocol. At 24 h post transfection, cells were harvested with PBS + 0.1% EDTA and resuspended at $6 \times 10^5$ cells/mL in DMEM 10% FCS. The cells were mixed in suspension at a 50/50 ratio and 100 µL were plated per well in a 96-well

plate (uClear, #655090). 30 min after plating, cells were imaged every 150 sec for 2.5 h at 37°C, 5% $CO_2$ on an Opera Phenix High-Content Screening System (PerkinElmer).

## Pseudovirus generation and infection

Pseudoviruses were produced by transfection of 293T cells as previously described[51]. Briefly, cells were cotransfected with plasmids encoding for lentiviral proteins, a luciferase reporter, and the HKU1 spike plasmid. Pseudotyped virions were harvested 2 and 3 days after transfection. Production efficacy was assessed by measuring infectivity or HIV Gag p24 concentration. For transfected cells (293T), infection was performed 24 h post-transfection, in suspension using 10 ng of p24 and $2 \times 10^4$ cells in 100 μL. For the stable cell lines, infection was performed on plated cells, with or without spinoculation (2 h at 2000 g), using 10–50 ng of p24 per well and $2 \times 10^4$ cells in 100 μL in a 96 well plate. The next day, 100 μL of media was added. 48 h post-infection, 100 μL of media was carefully removed, and 100 μL of BrightGlo™ lysis buffer (ProMega) was added. After 10 min, luminescence was acquired using the EnSpire in a white plate (PerkinElmer).

## Isolation and characterization of a live HKU-1 virus

**Origin of the sample—**Respiratory material of sample MAL21 0303 was obtained in the winter of 2022–2023 at Amsterdam UMC. Material was collected in Universal Transport Medium (Copan) and stored at −80°C. Details on the disease of the patient are unknown as material were donated for research anonymously. Presence of HCoV-HKU1 was determined via real time qPCR as described [52] with primers: HKU1 forward: 5'-TCCTACTAYTCAAGAAGCTATCC-3'; HKU1 reverse 5'-AATGAACGATTATTGGGTCCAC-3'; and HKU1-probe CY5 BHQ2 TYCGCCTGGTACGATTTTGCCTCA.

**HKU1 isolation and culture on Human nasal epithelium—**MucilAir™, reconstructed human nasal epithelium cultures that had been differentiated for 4 weeks were purchased from Epithelix (Saint-Julien-en-Genevois, France) and were cultured in 700 μL MucilAir™ media on the basal side of the air/liquid interface (ALI) cultures and monitored for healthy cilia movements. Cultures were kept at 34 °C under a 5% $CO_2$ atmosphere. One-hour prior to infection, mucus was removed from the apical side of the culture by washing with HBSS (Gibco). For viral isolation, cells were infected with nasal swabs diluted at a 1:4 ratio in universal transport medium (Copan) for 2 h at 34°C. Viral input was removed and cells were washed three times with 200 μL of HBSS (Gibco). Apical side was harvested twice every 24 h for 7 days by adding 200 μL HBSS for 10 min at 34°C and collecting the liquid on the apical side and diluting it (1:1) in virus transport medium (Copan). The harvest was centrifuged at 1000 g for 5 min to remove debris, 50 μL was used for qPCR and the remaining samples were stored at −80°C. Passage 1 (P1) and P2 viral stocks were sequenced with identical results.

**Sequencing of the HKU1 strain—**RNA was extracted from the cell supernatant using the QIAamp Viral RNA kit (Qiagen) following the manufacturer instructions. Extracted RNA was treated with Turbo DNase (Ambion) followed by ribosomal RNA[53]. RNA was reverse-transcribed into double stranded cDNA using random hexamers,

and libraries prepared using the Nextera XT kit (Illumina), before sequencing on an Illumina NextSeq500 (2 × 75 cycles). Raw sequence data (human reads removed) were deposited in the European Nucleotide Archive (ENA) portal (https://www.ebi.ac.uk/ena/) under bioproject accession number PRJEB64017. To determine the sequence of the acidic tandem repeat region of the genome, the region was amplified using external primers (HKU1_ATR_L1 5'-ATGAAGCAATGGCCTCTCGT-3' and HKU1_ATR_R1 5'-CACAGAACGCAACCAACAGT-3'), before Sanger sequencing.

**Genome assembly—**Adapters and low-quality sequences of raw reads were removed using Trimmomatic v0.39[54]. We assembled the trimmed reads using megahit v1.2.9[55] with default parameters. The contigs were queried against the NCBI non-redundant protein database using DIAMOND v2.0.4[56], to look for potential contaminants in addition to the detected HKU1 genome. The Sanger data was used with the assembled contigs to generate the final HKU1 scaffold, on which the trimmed reads were mapped to generate the final consensus (Extended Data Fig. 8). The mapping data was visually checked to confirm the accuracy of the obtained genome using Geneious Prime 2023. The sequence of the isolated virus was deposited in GenBank, ID: HCoV-HKU1/NDL/IPP01/2022, accession number OR260091.

**Phylogenetic and recombination analysis—**All available complete HKU1 genome sequence data and metadata were retrieved from BV-BRC (PMID: 36350631) (https://www.bv-brc.org/) in June 2023. Sequences were aligned using MAFFT (v.7.467)[57] and the alignment was checked for accuracy using BioEdit v7.2.5. We used a combination of six methods implemented in RDP4[58] (RDP, GENECONV, MaxChi, Bootscan, SisScan, and 3SEQ) to detect potential recombination events in the newly reported genome. The ModelFinder application[59], as implemented in IQ-TREE v2.0.6 (PMID: 25371430), was used to select the best-fitting nucleotide substitution model, and maximum-likelihood phylogenies were inferred using complete genomes or the spike coding sequences. Branch support was calculated using ultrafast bootstrap approximation with 1000 replicates[60]. The phylogenies were visualized using the auspice module from Nextstrain[61]. Interactive phylogenies are available at: https://github.com/Simon-LoriereLab/HKU1

## Analysis of HKU-1 replication by RT qPCR

Viral RNA was extracted from culture supernatants using the Quick-DNA/RNA Viral 96 Kit (Zymo) according to manufacturer's instructions. qPCR was run using the Luna Universal Probe One-Step kit on a QuantStudio6 (Thermo) according to manufacturer's instructions using the following primers (HKUqPCR5: 5'-CTGGTACGATTTTGCCTCAA-3') and (HKUqPCR3: 5'-ATTATTGGGTCCACGTGATTG-3')[29] and TaqMan™ QSY probe (5'FAM-TTGAAGGCTCAGGAAGGTCTGCTTCTAA-QSY7–3'). A DNAString was used for generating a standard curve (5'-GGATCCTACTATTCAAGAAGCTATCCCTACTAGGTTTTCGCCTGGTACGATTTTGCCTCAAGGCTATTATGTTGAAGGCTCAGGAAGGTCTGCTTCTAATAGCCGGCCAGGTTCACGTTCTCAATCACGTGGACCCAATAATCGTTCATTAAGTAGAAGTAATTCTAATTTTAGACATTCTGATTCTATAGTGAAACCTG-3')

### Human nasal epithelium VHH inhibition experiments

One hour prior to infection, mucus was removed from the apical side of the culture by washing with HBSS (Gibco). For viral infectivity assays, cells were incubated for 30 min with 50 µL of universal transport media (Yocon), containing monomeric non-target VHH93 (also termed N-G9–3[62]) or anti-TMPRSS2 VHH A07 at 5 µM. Then $5\times10^6$ viral copies were added in 50 µL of universal transport medium for 2 h at 34°C (final VHH of concentration 2.5 µM). Viral input was removed and cells were washed three times with 200 µL of HBSS (Gibco). After 48 h, cells were fixed on the apical and basal sides with 4% PFA for 30 min. For imaging, fixed cells were stained intracellularly with mAb10 at 1 µg/mL a pan anti-coronavirus spike antibody[30], anti-TMPRSS2 VHH-A01-Fc at 6 µg/mL and phalloidin Atto-647 (Sigma-aldrich) at 1:200 as described previously[63] and imaged using the LSM-700 confocal microscope (Zeiss).

### Image quantification

To quantify the effect of the nanobodies on HKU1 infection of epithelia, the fluorescence intensity of spike positive pixels of 5 fields (160 $\mu m^2$ each) spread over the surface of the sample was measured using ImageJ-Fiji.

### CRISPR-Cas9 knock-out

crRNAs TMPRSS2 (CGGATGCACCTCGTAGACAG) and pre-designed unspecific crRNA used as control were ordered from Integrated DNA Technologies, IDT. crRNA and tracrRNA were resuspended in IDT Duplex Buffer according to the manufacturer's instructions. On the day of the nucleofection, duplexes were formed by mixing equimolar concentration of crRNA and tracrRNA, followed by 5-min annealing at 95°C. 100 pmol of RNA duplexes were then mixed (1:2) with 50 pmol TrueCut™ Cas9 Protein v2 (Thermo Fisher Scientific) for 10 min at RT to generate ribonucleoprotein (RNP) complexes. Caco2 were resuspended in SE cell line buffer Solution (Lonza), mixed with RNP and Alt-R® Cas9 Electroporation Enhancer (90 pmol, IDT), and nucleofected in a 4D-Nucleofector™ System (Lonza) using the SE Cell line 4D-Nucleofector™ X Kit S (program DG-113). After nucleofection, cells were seeded in DMEM 10% FBS. 48 h post transfection, cells were subcloned. Clones were screened for TMPRSS2 knock-out by staining using VHH-A01-Fc and flow cytometry (immunostaining section). Knock out was confirmed by PCR and sequencing the target region using the following primers: forward (5'-AAGACGGAGGAGAAGGGTCA-3') and reverse (5'AGTTGTAGACACCTAGGGAGAA-3').

### Protein production

**Construct design—**Spike, RBD, TMPRSS2 and ACE2 constructs were obtained from Genscript as codon-optimized synthetic genes. Ectodomains from HKU1A (residues 14–1281) and B (residues 14–1276) were cloned into pcDNA3.1(+), downstream of a murine Ig kappa signal peptide (METDTLLLWVLLLWVPGSTG) and upstream of a thrombin cleavage site followed by a His-tag. Spikes were stabilized by mutating the furin cleavage site ($^{756}$RRKRR$^{760}$>$^{756}$GGSGS$^{760}$ in HKU1A; $^{752}$RRKRR$^{756}$>$^{752}$GGSGS$^{756}$ in HKU1B;), two residues in the S2 subunit ($^{1071}$AL$^{1072}$>$^{1071}$PP$^{1072}$ in HKU1A; $^{1067}$NL$^{1068}$>$^{1067}$PP$^{1068}$

in HKU1B) and adding a Foldon trimerization motif at the C-terminus. The ectodomain from the Wuhan SARS-CoV-2 Spike (residues 1–1208) was cloned into pcDNA3.1(+) and was stabilized with 6 proline mutations (F817P, A892P, A899P, A942P, K986P, V987P), as reported[64]. The furin site was also replaced as above ($^{682}$RRAR$^{685}$>$^{682}$GSAS$^{685}$), a C-terminal Foldon motif was introduced, as well as Hisx8, Strep, and Avi tags.

The RBDs (residues 323–609 for HKU1A; 323–607 for HKU1B; 331–528 for SARS-CoV-2 Wuhan) were cloned into pCAGGS (HKU1) or pcDNA3.1(+) (SARS-CoV-2), following a murine immunoglobulin kappa signal peptide, and upstream of a thrombin cleavage site and *intandem* Hisx8, Strep and Avi-tags. The WT TMPRSS2 ectodomain (residues 107–492) followed by C-terminal tags (8xHis-tag and AviTag) was synthesized and cloned into pcDNA3.1/Zeo(+) expression vector (Thermo Fisher Scientific). The TMPRSS2 ectodomain with the S441A mutation was cloned into a modified pMT/BiP plasmid (Invitrogen; hereafter termed pT350), which translates the protein in frame with an enterokinase cleavage site and a double strep-tag at the C-terminal end. The ACE2 peptidase domain (residues 19–615) was cloned in pcDNA3.1(+) with a murine immunoglobulin kappa signal peptide and a C-terminal thrombin cleavage site followed by a Strep-tag. The coding sequences of the selected VHHs in the vector pHEN6 were subcloned into a bacterial expression vector pET23 encoding a C terminal His-tag using NcoI and NotI restriction sites.

**Protein expression and purification—**RBD, spike and ACE2-encoding plasmids were transiently transfected into Expi293F™ cells (Thermo-Fischer) using FectoPro DNA transfection reagent (PolyPlus) or polyethylenimine (PEI) precipitation method, as previously described[65]. After 5 days at 37 °C, cells were harvested by centrifugation and the supernatants were concentrated. The spike proteins used for flow cytometry were purified from culture supernatants by high-performance chromatography using the Ni Sepharose Excel Resin according to the manufacturer's instructions (GE Healthcare) and dialyzed against PBS using Slide-A-Lyzer dialysis cassettes (Thermo Fisher Scientific). The spike proteins used for ELISA were further purified by size-exclusion chromatography (SEC) on a Superose6 10/300 column (Cytiva). Eluted fractions were analyzed by SDS-PAGE and those containing bands of the expected molecular weight were pooled, concentrated and further purified by SEC on a Superdex 200 10/300 column (Cytiva). AviTagged SARS-CoV-2 tri-S used for flow cytometry was biotinylated using Enzymatic Protein Biotinylation Kit (Sigma-Aldrich). HKU1A and HKU1B spike proteins used for ELISA were biotinylated using EZ-Link™ Sulfo-NHS-biotinylation kit (Thermo Fisher Scientific). The HKU1B RBD used for the BLI experiment with nanobodies was biotinylated with the BirA biotin-protein ligase standard reaction kit (Avidity).

The pT350 plasmid encoding S441A TMPRSS2 was used to perform a stable transfection on *Drosophila* S2 cells with the pCoPuro plasmid for puromycin selection. The cell line was selected and maintained in serum-free insect cell medium (HyClone, GE Healthcare) containing 7 μg/mL puromycin and 1% penicillin/streptomycin. For protein production, the cells were grown in spinner flasks until the density reached $10^7$ cells/mL, at which point the protein expression was induced with 4 μM $CdCl_2$. After 6 days, the culture was centrifuged and the supernatant was concentrated and used for affinity purification using a Streptactin

column (IBA). The eluate was concentrated and applied onto a Superdex 200 16/60 column (Cytiva) equilibrated with 10 mM Tris-HCl (pH 8.0), 100 mM NaCl.

E. coli BL21pLysS cells were transformed with the plasmids encoding the different VHHs, which were expressed in the cytoplasm after overnight induction with 0.5 mM IPTG at 16°C. The cultures were centrifuged, the bacterial pellets were resuspended in 40 mL of lysis buffer (20 mM Tris-HCl, 200 mM NaCl, 20 mM imidazole, pH 8.0) containing complete protease inhibitor cocktail (Roche) and they were frozen at −80°C until used. On the purification day, the resuspended pellets were thawed, sonicated (15 min, 9s on-pulse, 5s off-pulse), centrifuged and loaded onto a HisTrap column. Bound proteins were eluted with a linear gradient of buffer B (20 mM Tris-HCl, 200 mM NaCl, 500 mM imidazole, pH 8.0) and analyzed by SDS-PAGE. Fractions with higher purity were pooled, concentrated and further purified by SEC on a Superdex 75 16/60 column (Cytiva) pre-equilibrated in 10 mM Tris-HCl, 100 mM NaCl, pH 8.0.

The purity of the final protein samples was analyzed by SDS-PAGE followed by Coomasie Blue staining or silver staining. For gels, see SI 2.

## Flow cytometry

For Spike binding, 293T cells were transiently transfected with TMPRSS2 and maintained in the presence or absence of Camostat (10 μM) for 24 h. The cells were incubated with soluble biotinylated spike diluted in MACS buffer (PBS, 5 g/L BSA, 2 mM EDTA) at 2 μg/mL for 30 min at 4°C. The cells were then washed twice with PBS and then incubated with Alexa Fluor 647-conjugated streptavidin (Thermo Fisher Scientific, S21374, 1:400) for 30 min at 4°C. The cells were washed once with PBS and fixed with 4% paraformaldehyde. The results were acquired using an Attune Nxt Flow Cytometer (Life Technologies, software v3.2.1). Transfection efficiency for TMPRSS2 was assessed by using either a commercial anti-TMPRSS2 antibody (for the experiments performed at the initiation of the study), the anti-TMPRSS2 monomeric VHH or the dimeric VHH A01-Fc (see below).

The staining with the commercial anti-TMPRSS2 antibody was performed on fixed cells by staining intracellularly with rabbit anti-TMPRSS2 (Atlas HPA035787), for 30 min at RT in PBS/BSA/Azide/0.05% Saponin followed by a Alexa Fluor 647 Goat anti-Rabbit antibody (Thermo Fisher Scientific, A-21245, 1:500).

For the spike, transfection efficiency was measured at the surface of live cells using mAb10 diluted in MACS buffer for 30 min at 4°C, and a human secondary IgG. mAb10 is an antibody generated from a SARS-CoV-2 infected patient which cross-reacts with HKU1[30].

Surface expression of TMPRSS2 was assessed on live cells by staining with anti-TMPRSS2 VHH-A01-Fc (described in the study) at 1 μg/mL, for 30 min at 4°C in MACS buffer, followed by staining with Alexa Fluor 647-conjugated Goat anti-Human antibody (Thermo Fisher Scientific, A-21445, 1:500). The control VHH Fc ctrl (R3VQFc) recognizes an unrelated protein (phosphorylated Tau protein)[62].

The monomeric VHHs were used at 0.5 μg/mL in MACS buffer for 30 min at 4°C, staining was revealed using a coupled anti-His antibody (R&D Systems, IC0501R, 1:1000).

Transfection efficiency for myc-tagged constructs was assessed on fixed cells by staining intracellularly with mouse anti-c-myc antibody, clone 9E10 (Thermo - M4439), for 30 min at RT in PBS/BSA/Azide/0.05% Saponin followed by an Alexa Fluor 647-conjugated Goat anti-Mouse antibody (Thermo Fisher Scientific, A-21242, 1:500). Transfection efficiency of APN (CD13) and DPP4 (CD26) was assessed on live cells by surface staining in MACS buffer with CD13-PE (130–120-312, Miltenyi Biotec, 1:50) and CD26-PE (130–126-41, Miltenyi Biotec, 1:50) for 30 min at 4°C. The cells were washed twice with PBS and fixed with 4% paraformaldehyde. The results were acquired using an Attune Nxt Flow Cytometer (Life Technologies). Gating strategies are described in SI 3.

### Sialic acid staining

Cells were harvested using PBS/0.1% EDTA for 5 min at 37°C, washed in PBS and stained 1 h at 4°C in PBS/1% SVF containing either 10 μg/mL Sambucus Nigra Lectin-FITC (Lectin NSA) (L32479 – Thermo) or 2.5 μg/mL recombinant mouse Siglec E-Fc (551504 – BioLegend). Cells were washed twice in PBS. Lectin-stained cells were fixed for 10 min in 4% paraformaldehyde. Siglec-E-Fc stained cells were further incubated with Alexa Fluor 647-conjugated Goat anti-Human antibody (Thermo Fisher Scientific, A-21445, 1:500) for 30 min at 4°C before being fixed for 10 min in 4% paraformaldehyde.

### ELISA assay

ELISAs were performed as previously described[66]. Briefly, high-binding 96-well ELISA plates (Costar; Corning) were coated overnight with 250 ng/well of purified TMPRSS2 or ACE2. After washing with 0.05% Tween 20-PBS (washing buffer), the plates were blocked for 2 h with 2% BSA, 1 mM EDTA, 0.05% Tween 20-PBS (Blocking buffer), washed, and incubated with serially diluted soluble biotinylated spike proteins. Recombinant spike proteins were tested at 100 μg/mL, and at 7 consecutive 1:2 dilutions in PBS. After washings, the plates were revealed by incubation for 1 h with HRP-conjugated streptavidin (BD Biosciences) in blocking buffer and by adding 100 μL of HRP chromogenic substrate (ABTS solution, Euromedex) after washing steps. Optical densities were measured at 405 nm ($OD_{405nm}$) and background values given by incubation of PBS alone in coated wells were subtracted. Experiments were performed using HydroSpeed microplate washer and Sunrise microplate absorbance reader (Tecan).

### BLI assay

Affinity of recombinant RBDs towards the purified ectodomains of S441A TMPRSS2 or ACE2 was assessed in real-time using a bio-layer interferometry Octet-Red384 device (Pall ForteBio). Nickel-NTA capture sensors (Sartorius) were loaded for 10 min at 1000 rpm shaking speed with the Wuhan RBD at 100 nM or the HKU1A/B RBDs at 200 nM in PBS. The sensors were then blocked with PBS containing BSA at 0.2 mg/mL (assay buffer) and were incubated at 1000 rpm with two-fold serially diluted concentrations (800 nM to 3.12 nM) of S441A TMPRSS2 or ACE2 ectodomains in assay buffer. Association and dissociation were monitored for 300 s and 240 s, respectively. Measurements for a reference sensor were recorded using a sensor loaded with an unrelated protein (CD147) that was dipped at each analyte concentration. A sample reference measurement was recorded from a sensor loaded with either RBD and dipped in the assay buffer. Specific signals

were calculated by double referencing, substracting nonspecific signals obtained for the sensor and sample references from the signals recorded for the RBD-loaded sensors dipped in S441A TMPRSS2 solutions. The steady-state signal was plotted against the analyte concentration and the curve was fitted assuming a 1:1 binding model.

The affinity of the nanobodies for the S441A TMPRSS2 ectodomain was determined using a similar procedure. Nickel-NTA capture sensors were loaded with each nanobody at 100 nM in PBS, then blocked with assay buffer and incubated at 1000 rpm with two-fold serially diluted concentrations (400 nM to 3.12 nM) of S441A TMPRSS2. Association and dissociation were monitored for 240 s and 180 s, respectively. A sample reference measurement was recorded from a sensor loaded with each nanobody and dipped in the assay buffer. Association and dissociation profiles were fitted assuming a 1:1 binding model.

Experiments to identify anti-TMPRSS2 nanobodies that block binding to the HKU1 RBD were performed by immobilizing the biotinylated HKU1B RBD on Streptavidin capture sensors. They were blocked in assay buffer and dipped into solutions containing a pre-incubated mixture of TMPRSS2 S441A (200 nM) and a nanobody (400 nM). The signal corresponding to the association was recorded.

### TMPRSS2 enzymatic activity

Enzymatic activity was measured using BOC-QAR-AMC (R&D Systems, ES014), a substrate of TMPRSS2 that fluoresces when cleaved. For wild type and mutant TMPRSS2, cells were transfected in a black bottom 96 well plate as described above. After 24 h, media was replaced with 100 μL FCS free, phenol red free media, containing 100 μM of fluorogenic substrate. Indicated concentration of inhibitors were added. When the assay was performed with soluble TMPRSS2, 60 nM of soluble protein was added to the well and mixed with VHH nanobodies for 15 min, before adding 100 μM of fluorogenic substrate.

### Western Blot

Cells were lysed in TXNE buffer (1% Triton X-100, 50 mM Tris–HCl (pH 7.4), 150 mM NaCl, 5 mM EDTA, 1X Roche cOmplete protease inhibitors) for 30 min on ice. Equal amounts (10 μg) of cell lysates were analyzed by Western blot. The following antibodies were diluted in WB buffer (PBS, 1% BSA, 0.05% Tween, 0.01% Na Azide): rabbit anti-human TMPRSS2 (Atlas antibodies cat# HPA035787, 1:1,000), mouse anti-beta actin (Abcam, 60008–1-Ig, 1:2,000), rabbit anti-HKU1 S1 polyclonal antibody (Thermofisher Scientific Cat #PA5–120768, 1:2,000) and rabbit anti-HKU1 S2 polyclonal antibody (Thermofischer Scientific #PA5–120769, 1:1,000). Species-specific secondary DyLight-coupled antibodies were used (1:10,000) and proteins were revealed using a Licor Imager. Images were processed using Image Studio Lite software v5.2.5.

## Nanobody isolation and production

### Alpaca immunization

Animal procedures were performed according to the French legislation and in compliance with the European Communities Council Directives (2010/63/UE, French Law 2013–118,

February 6, 2013). The Animal Experimentation Ethics Committee of Pasteur Institute (CETEA 89) approved this study (2020–27412). One young adult male alpaca (Lama pacos) was immunized at days 0, 17, and 24 with 150 μg of S4441A TMPRSS2. The immunogen was mixed with Freund complete adjuvant for the first immunization and with Freund incomplete adjuvant for the following immunizations. The immune response was monitored by titration of serum samples by ELISA on coated TMPRSS2. The bound alpaca antibodies were detected with polyclonal rabbit anti-alpaca IgGs[67].

### Library construction and phage display

The blood of the immunized animal (about 300 mL) was collected and peripheral blood lymphocytes were isolated by centrifugation on a Ficoll (Cytiva, Velizy, France) discontinuous gradient and stored at −80°C until further use. Total RNA and cDNA were obtained as previously described[67]. The VHH repertoires were amplified from the cDNA by two successive PCR reactions and the VHH fragments were cloned into the SfiI/NotI restriction sites of pHEN6 phagemid vector[62]. The selection of specific phage-VHHs was performed by phage display. A large number of phage-VHHs ($10^{13}$) was used to perform 3 rounds of panning. Briefly, Phage-VHHs were incubated for 1 h with TMPRSS2 that has been previously coated on an immunotube (Nunc). To remove non-specific binders, an extensive washing procedure was performed and specific phage-VHHs were eluted in 100 mM triethylamine (TEA). *E.coli* TG1 at exponential growth phase were then infected with eluted phage-VHHs. Phage-VHHs were produced from individual colonies and binding of the phages to TMPRSS2 on plate was revealed with an anti-M13 monoclonal antibody conjugated to peroxidase (Abcam). The VHH nucleotide sequences were determined using M13–40 primer (Eurofins, Ebersberg, Germany).

### Production of VHHs

The coding sequences of the selected VHHs in the vector pHEN6 were subcloned into a bacterial expression vector pET23 encoding a C terminal His tag using NcoI and NotI restriction sites. Sequences of the VHH are available in SI 4. Transformed *E. coli* BL21pLysS cells expressed VHHs in the cytoplasm after overnight induction with 0.5 mM IPTG at 16°C. Purified VHHs were isolated on Co++ affinity columns from cytoplasmic extracts treated by 10 U/mL Benzonase Nuclease (Merck) and Complete protease inhibitor (Roche), according to the manufacturer's instructions, followed by size exclusion chromatography (SEC) with a Superdex 75 column (Cytiva).

### Production of dimeric VHH-Fc

VHHs' engineered genes were cloned into a pFUSE-derived vector (InvivoGen); this vector harbors a human IgG1-Fc domain. Consequently, the VHH was expressed as a Fc-fusion bivalent antibody. The vector was used to transform Expi293F mammalian cells (ThermoFisher), and protein expression was carried out according to manufacturer's recommendations. Protein was purified from the expression medium by affinity chromatography on a 1 mL protein G column (Cytiva). After sample application, the column was washed with 20 column volumes of PBS and the protein was subsequently eluted with 10 column volumes of PBS supplemented with 0.1 M Glycine (pH=2.3). Affinity-eluted

VHH-Fc were finally polished on a HiLoad 16/600 Superdex 200pg Pre-packed column (Cytiva) using PBS buffer[68]

### Statistical analysis

Flow cytometry data were analyzed with FlowJo™ v10.8 software (BD Life Science). Calculations were all performed with Microsoft Excel 365. GraphPad Prism 9 for Mac was used to generate figures and for statistical analysis (GraphPad Software). Statistical significance between different conditions was calculated using the tests indicated in the corresponding figure legends.

### Illustrations

All illustrations were generated by using Inkscape. They can be re-used if cited properly.

## Extended Data

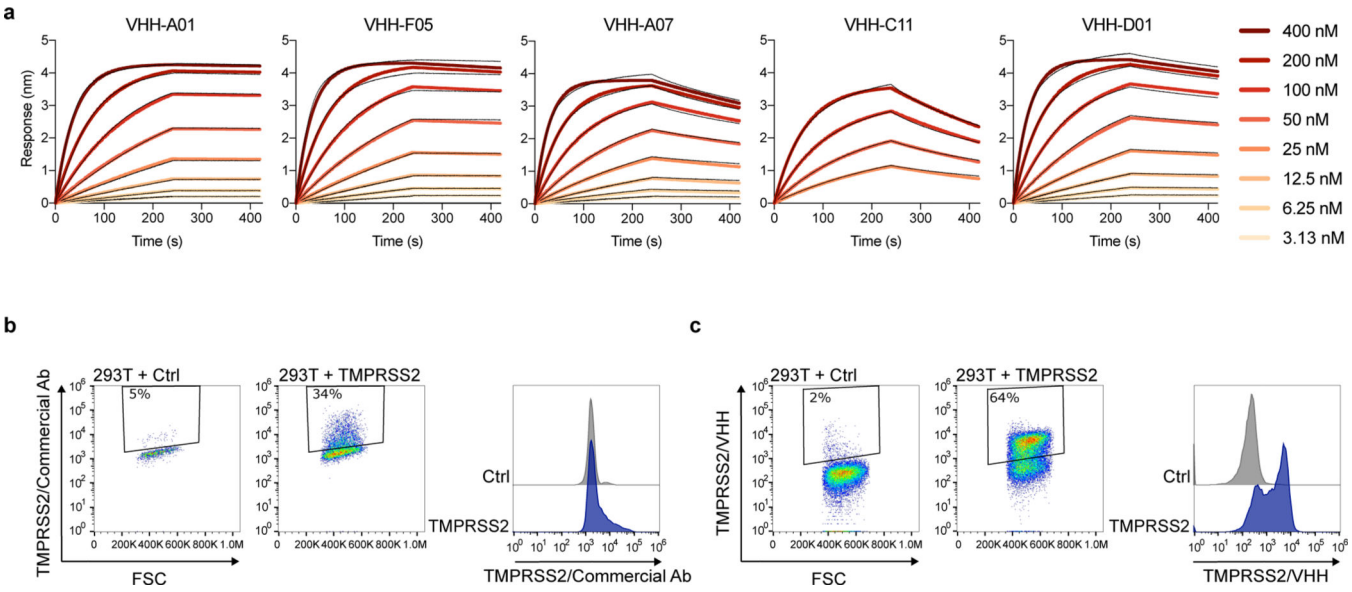


**Extended Data Figure 1.**

**a. Binding of the 5 anti-TMPRSS2 VHH on recombinant TMPRSS2 measured by BLI. b, c. Comparison of one commercial TMPRSS2 antibody and of the dimeric anti-TMPRSS2 VHH A01-Fc.** 293T cells were transfected with WT TMPRSS2. 24 h later, cells were analysed by flow-cytometry. Staining with the commercial antibody was performed on fixed cells **(b)** while surface staining with the VHH was performed on live cells **(c)**.

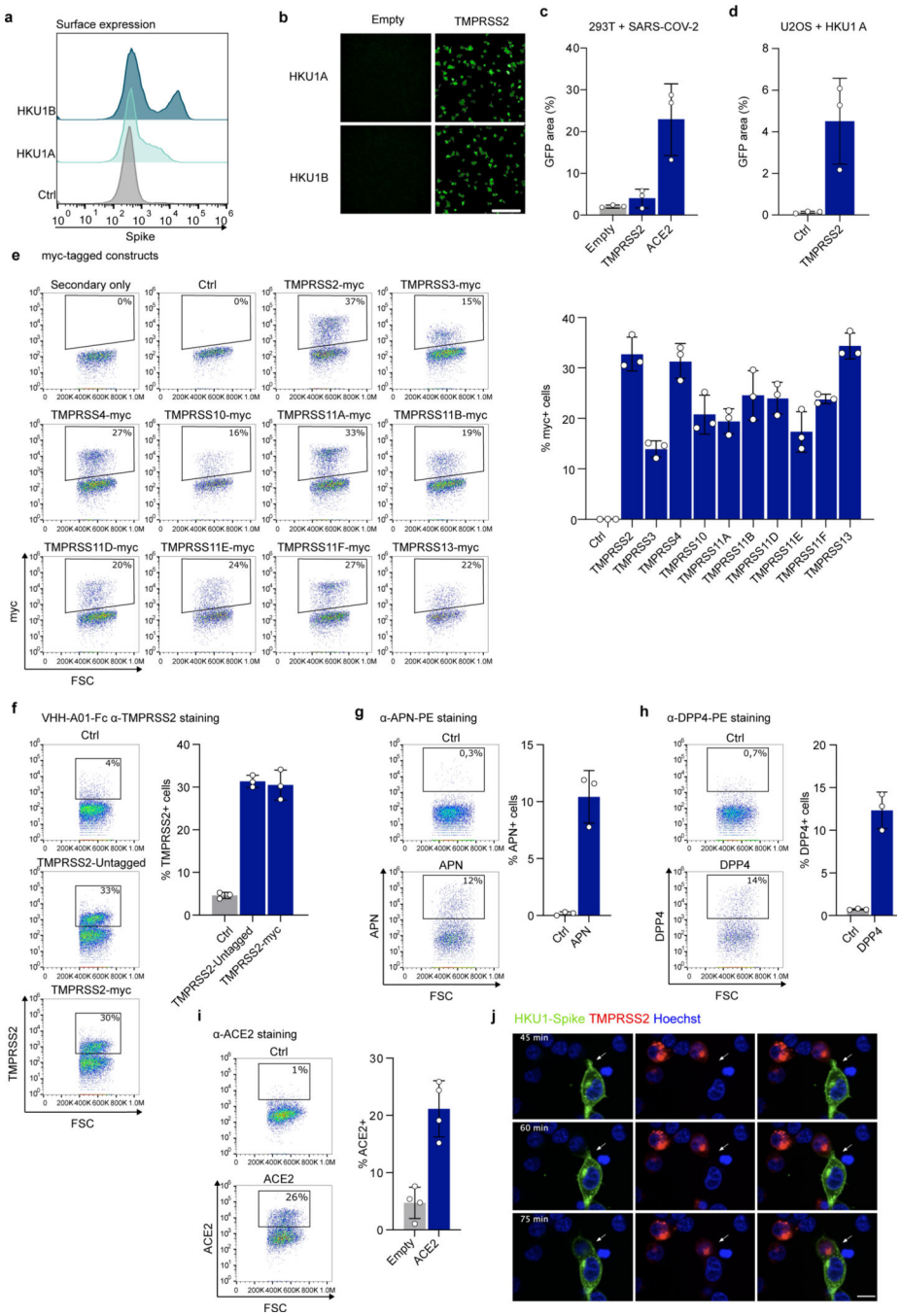


**Extended Data Figure 2. Effect of TMPRSS2 and other proteases on HKU1 cell-cell fusion. a, b. Surface expression and fusogenic activity of HKU1 spikes.**

**a.** 293T cells were transfected with plasmids encoding for HKU1A or HKU1B spikes and stained 24 h later with mAb10, a pan anti-coronavirus spike antibody. Data are representative of 3 independent experiments**. b.** Cell-cell fusion mediated by HKU1A or HKU1B spikes. 293T GFP-Split cells were transfected with HKU1 spikes and TMPRSS2, fusion was visualized by the appearance of GFP+ cells. Data are representative of 6 independent experiments. Scale bar: 400 $\mu$m **c. Cell-cell fusion mediated by the SARS-**

**CoV-2 spike.** 293T GFP-Split cells were transfected with SARS-CoV-2 spike, in the presence of ACE2 or TMPRSS2, fusion was visualized by the appearance of GFP+ cells. Data are mean ± SD of 3 independent experiments **d. U2OS cell-cell fusion mediated by HKU1A spike.** U2OS GFP-Split cells were transfected with HKU1A spike and TMPRSS2, fusion was visualized by the appearance of GFP+ cells 24 h later. Data are mean ± SD of 3 independent experiments. **e. Expression levels of myc-tagged proteases.** 293T cells were transfected with a control plasmid or the indicated myc-tagged TMPRSS constructs and stained 24 h later with myc antibody 9E10. Left: Representative dot plots. Right: Percentage of positive cells. Data are mean ± SD of 3 independent experiments. **f. Surface expression of tagged and untagged TMPRSS2.** 293T cells were transfected with WT TMPRSS2 (TMPRSS2-Untagged) or a myc-tagged TMPRSS2 and surface stained for TMPRSS2 using VHH-A01-Fc. Left: Representative dot plots. Right: Percentage of positive cells. Data are mean ± SD of 3 independent experiments. **g, h, i . Surface expression of APN, DPP4 and ACE2.** 293T cells were transfected with APN, DPP4 or ACE2 plasmids, and surface stained with the respective antibodies 24 h later. Left: Representative dot plots. Right: Percentage of positive cells. Data are mean ± SD of 3 (TMPRSS2, APN, DPP4) or 4 (ACE2) independent experiments. **j. Images of time lapse microscopy of HKU1-mediated cell-cell fusion** (extracted from Supp. video 1). 293T cells were transfected either with TMPRSS2-scarlet-I or HKU1A S-NeonGreen. After 24 h, cells were mixed and imaged every 2.5 min for 2 h at 37°C.

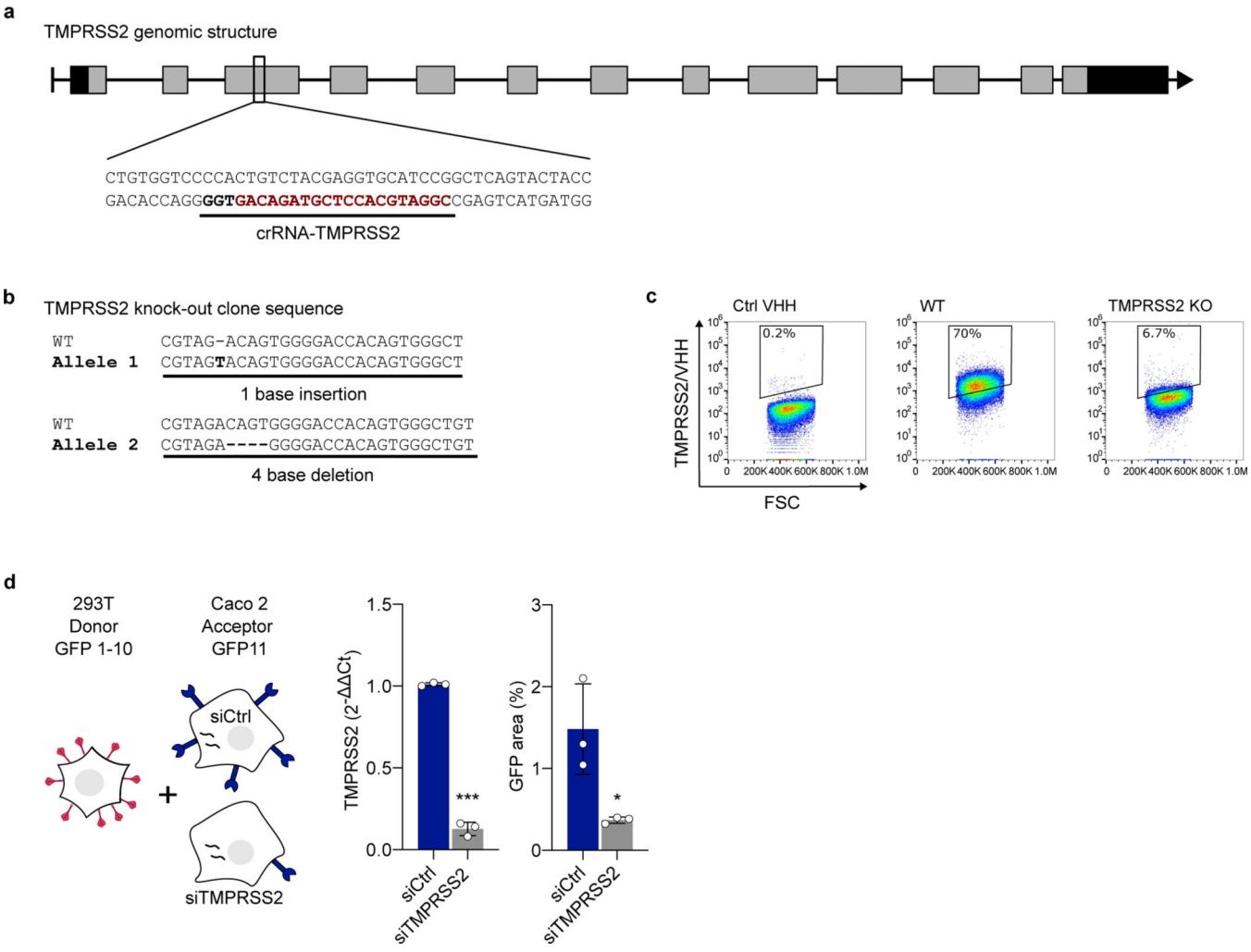


**Extended Data Figure 3. Knock-out and silencing of TMPRSS2 in Caco2 cells. a. Linear diagram of the organization of the TMPRSS2 gene.**

The CRISPR-Cas9 targeting site is underlined and the proto-spacer recognition motif (PAM) is in bold. Rectangles represent exons, black for 5' and 3' untranslated regions, gray for coding regions. **b. Sequence analysis of the knock-out Caco2 clone.** Both alleles compared to the original wild-type sequence are shown. The knock-out clone harbors an out-of-frame deletion and an insertion, resulting in a frameshift on both alleles. **c. Validation of TMPRSS2 knock-out by TMPRSS2 surface staining.** Representative dot plots of VHH anti-TMPRSS2 (VHH-A01-Fc) surface staining of a WT and KO Caco2 obtained following CRISPR gene targeting. **d. Role of endogenous TMPRSS2 on cell-cell fusion assessed by siRNA.** 293T donor cells expressing HKU1A spike were mixed with Caco2 acceptor cells, silenced or not for TMPRSS2. Left: experimental design. Middle: relative expression of TMPRSS2 in Caco2 cells, assessed by RT-qPCR. Data were normalized to *β-Tubulin* levels. Relative mRNA expression normalized to siCtrl condition ($2^{-\Delta\Delta CT}$) was plotted. Right: fusion was quantified by measuring the GFP area after 20 h of coculture. Data are mean ± SD of 3 independent experiments. Statistical analysis: two-sided unpaired t-test compared to siCtrl cells. ***p<0.0001.

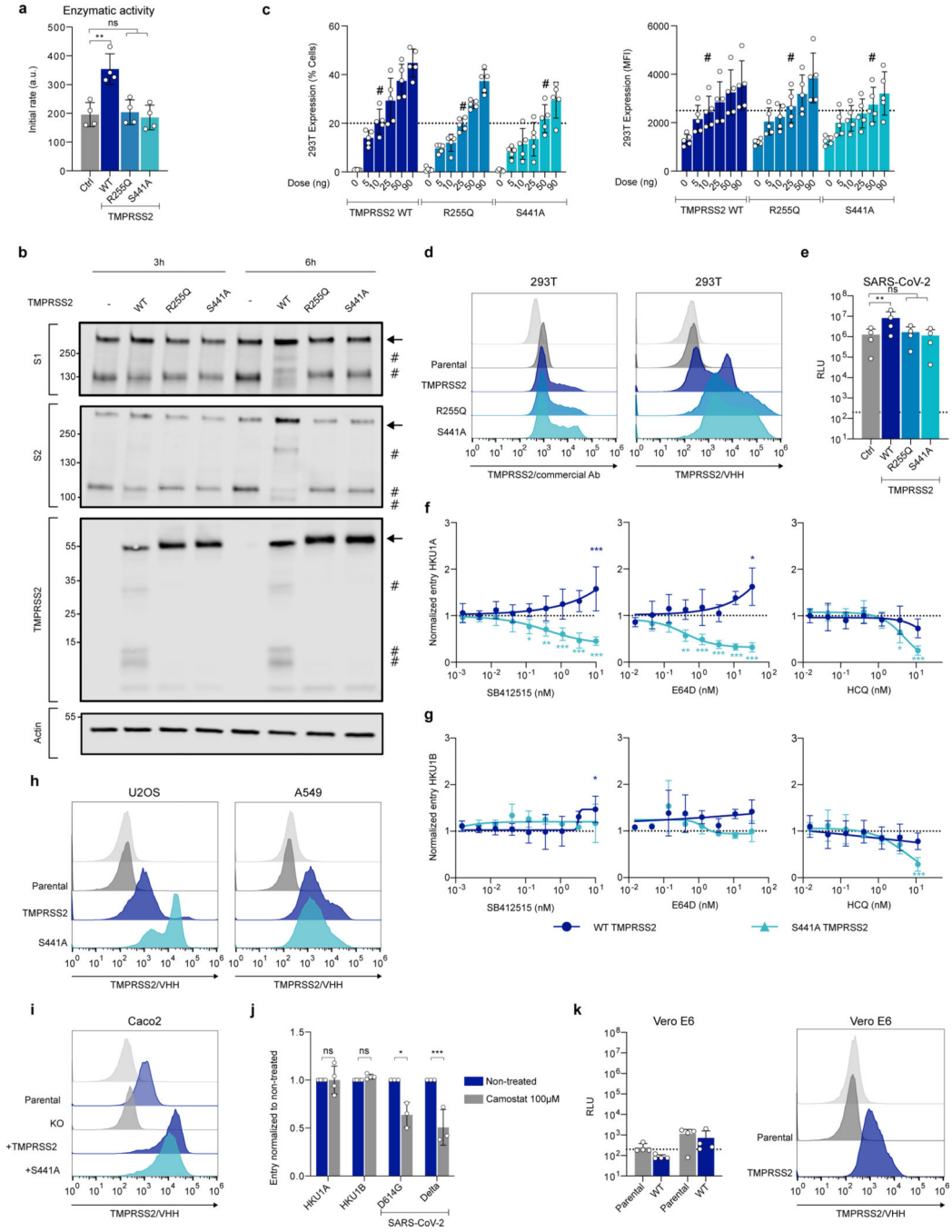


**Extended Data Figure 4. Effect of mutant TMPRSS2 on cell-cell fusion and pseudovirus infection a. Enzymatic activity of WT and mutant TMPRSS2.**

293T cells were transfected with WT and indicated TMPRSS2 mutants. 24 h post transfection, the catalytic activity was assessed using BoC-QAR-AMC fluorogenic substrate. Data are mean ± SD of 4 independent experiments. Statistical analysis: a: one-way ANOVA with Dunnett's multiple comparisons compared to Ctrl cells (transfected with pQCXIP-Empty). **p<0.01. **b. Effect of TMPRSS2 on HKU1 spike expressed on adjacent cells.** 293T cells were transfected either with HKU1A spike or with the

different TMPRSS2. 20 h post-transfection, cells were mixed at a 1:1 ratio, and let to settle. 3 or 6 h post-mixing, cells were harvested and lysed for WB. One membrane was probed for S1, TMPRSS2 and actin, another membrane was probed for S2 and actin. For gel source data, see SI 1c, d. Representative blots of 2. Molecular weights: kDa. The arrows and # denote the uncleaved and cleaved protein products, respectively. **c. Surface levels of WT and mutant TMPRSS2.** 293T cells were transfected with the indicated doses of TMPRSS2 plasmid. 18 h post-transfection they were stained intracellularly for TMPRSS2 using the commercial antibody. Left: % of TMP positive cells. Right: Median fluorescent intensity (MFI). #: indicates the chosen plasmid ratios to achieve similar TMPRSS2 levels with WT and indicated mutants. Data are mean ± SD of 3 independent experiments. **d. Comparison of the anti-TMPRSS2 commercial antibody and VHH staining in 293T cells.** 293T cells were transfected with WT, R255Q and S441A TMPRSS2 plasmids. Cells were stained 24 h later with the indicated antibodies and analysed by flow cytometry. One experiment representative of 3 is shown. Light grey curves correspond to staining with control antibodies or VHH. Parental: untransfected cells. **e. Effect of WT and mutant TMPRSS2 on SARS-CoV-2 pseudovirus infection.** 293T cells expressing ACE2 were transfected with WT and indicated TMPRSS2 mutants. 24 h later, cells were infected by Luc-encoding SARS-CoV-2 pseudovirus. Luminescence was measured after 48 h. Data are mean ± SD of 4 independent experiments. Statistical analysis: RM one-way ANOVA with Geisser-Greenouse correction on log-transformed data, with Dunnett's multiple comparisons compared to Ctrl cells (transfected with pQCXIP-Empty). **p<0.01. **f, g. Effect of SB412515, E64d or hydroxychloroquine (HCQ) on f. HKU1A or g. HKU1B pseudovirus infection**. 293T cells expressing WT or S441A TMPRSS2 were incubated for 2 h with the indicated drugs, before infection with HKU1A or HKU1B pseudoviruses. Luminescence was read 48 h post infection. Left: SB412515. Middle: E64d. Right: HCQ. Data are mean ± SD of 3 (E64d, HKU1B), 4 (E64d HKU1A, SB142515 HKU1B), 5 (HCQ HKU1A) or 6 (HCQ HKU1B, SB412515 HKU1A) independent experiments. Statistical analysis: RM two-way ANOVA with Geisser-Greenouse correction on non-normalized log transformed data, with Dunnett's multiple comparisons compared to the non-treated conditions. **h, i. Surface levels of TMPRSS2 in different cell lines stably expressing WT or S441 TMPRSS2.** Cells were stained for TMPRSS2 using VHH-A01-Fc and analyzed by flow cytometry. Representative histograms are shown. **h.** Left: U2OS. Right: A549. Light grey: cells stained with a non-target control VHH-Fc. Dark grey: Unmodified parental cell lines. Dark and light blue: Cells transduced with either TMPRSS2 or TMPRSS2 S441A mutant. **i.** Caco2. Light grey: cells stained with a non-target control VHH-Fc. Blue: Unmodified parental cell line. Dark Grey: TMPRSS2 KO Caco2. Dark and light blue: TMPRSS2 KO caco2 stably transduced with TMPRSS2 WT or S441A mutant expression vectors. **j. Effect of Camostat on endogenous TMPRSS2 in Caco2 cells.** Caco2 cells were incubated in the presence of 100 μM Camostat for 2 h, before infection with HKU1A, HKU1B, or SARS-CoV-2 (D614G or Delta) pseudovirus. Data are normalized to the infection in the absence of the drug. Data are mean ± SD of 3 (SARS-CoV-2) or 4 (HKU1) independent experiments. Statistical analysis: RM two-way ANOVA on non-normalized log transformed data, with Sidak's multiple comparisons compared to the non-treated conditions. **k. Susceptibility of Vero E6 and Vero E6-TMPRSS2 cells to HKU1 pseudovirus infection.** Left: pseudovirus infection. Right: TMPRSS2 surface levels.

Dark grey: Parental cells. Dark blue: Cells transduced with TMPRSS2. Data are mean ± SD of 4 independent experiments.

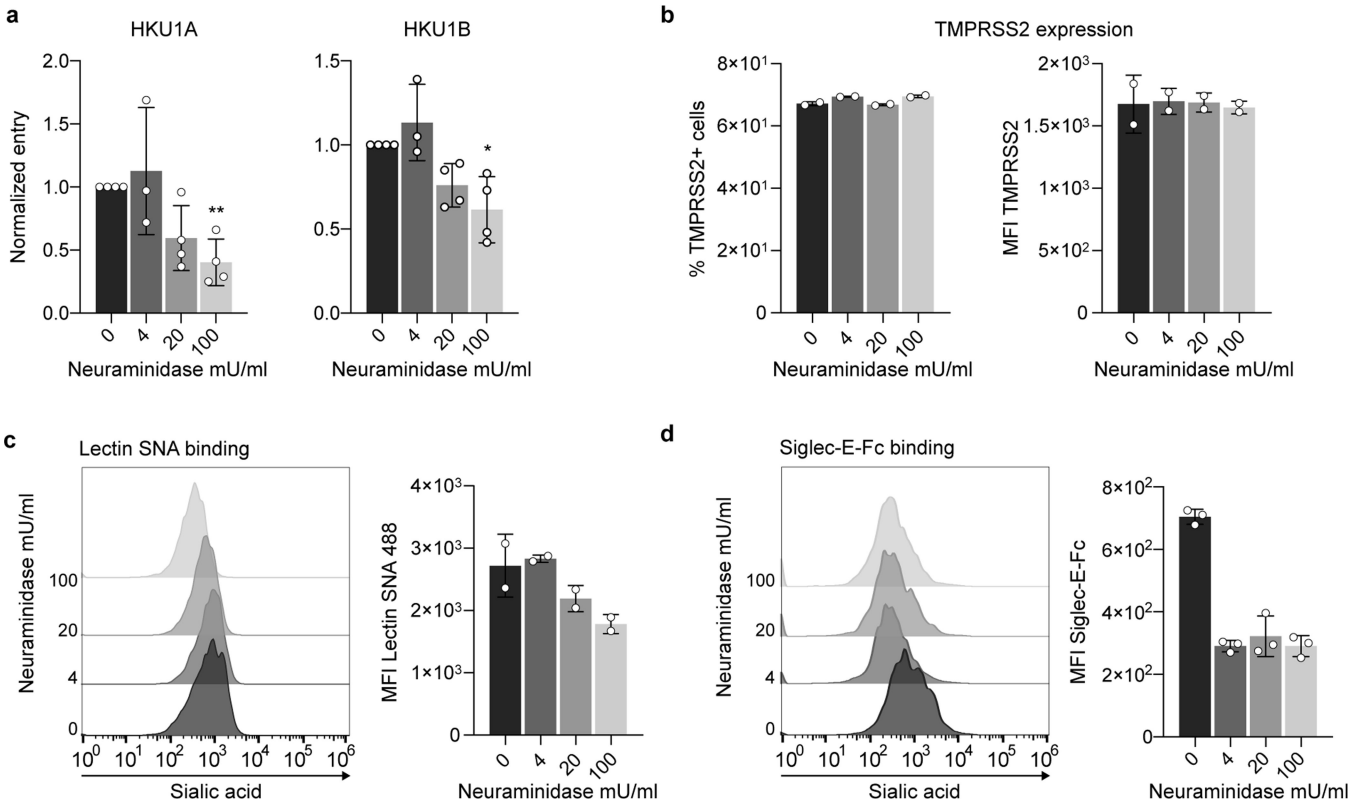


**Extended Data Figure 5. Effect of neuraminidase on HKU1 pseudovirus infection.**

U2OS-TMPRSS2 cells were treated with indicated concentration of neuraminidase from *Arthrobacter ureafaciens* for 24 h**. a. HKU1A and HKU1B pseudovirus infection in neuraminidase treated cells.** Cells were infected with HKU1 A or B pseudoviruses. Luminescence was read 48 h post infection. Data were normalized to the non-treated condition. Data are mean ± SD of 3 (4 mU/mL) or 4 (0, 20, 100 mU/mL) independent experiments. Statistical analysis: Mixed-effect analysis with Geisser-Greenhouse corrections (handles missing values) on non-normalized log transformed data, with Dunnett's multi-comparison test compared to non-treated cells. **b. Surface levels of TMPRSS2 in neuraminidase treated cells.** Left: % of TMP positive cells. Right: Median fluorescent intensity (MFI). Data are mean of 2 independent experiments. **c. Sambucus Nigra Lectin (SNA) binding on neuraminidase treated cells.** Treated cells were stained with fluorescent Lectin SNA which preferentially binds α2,6- over α-2,3 linked sialic acids. Left: Representative histograms. Right: MFI. Data are mean of 2 independent experiments. **d. Siglec-E binding on neuraminidase treated cells.** Treated cells were stained with recombinant Siglec-E-Fc protein which preferentially binds α2,8- over α2,3- and α2,6-linked sialic acids. Left: Representative histograms. Right: MFI. Data are mean ± SD of 3 independent experiments.

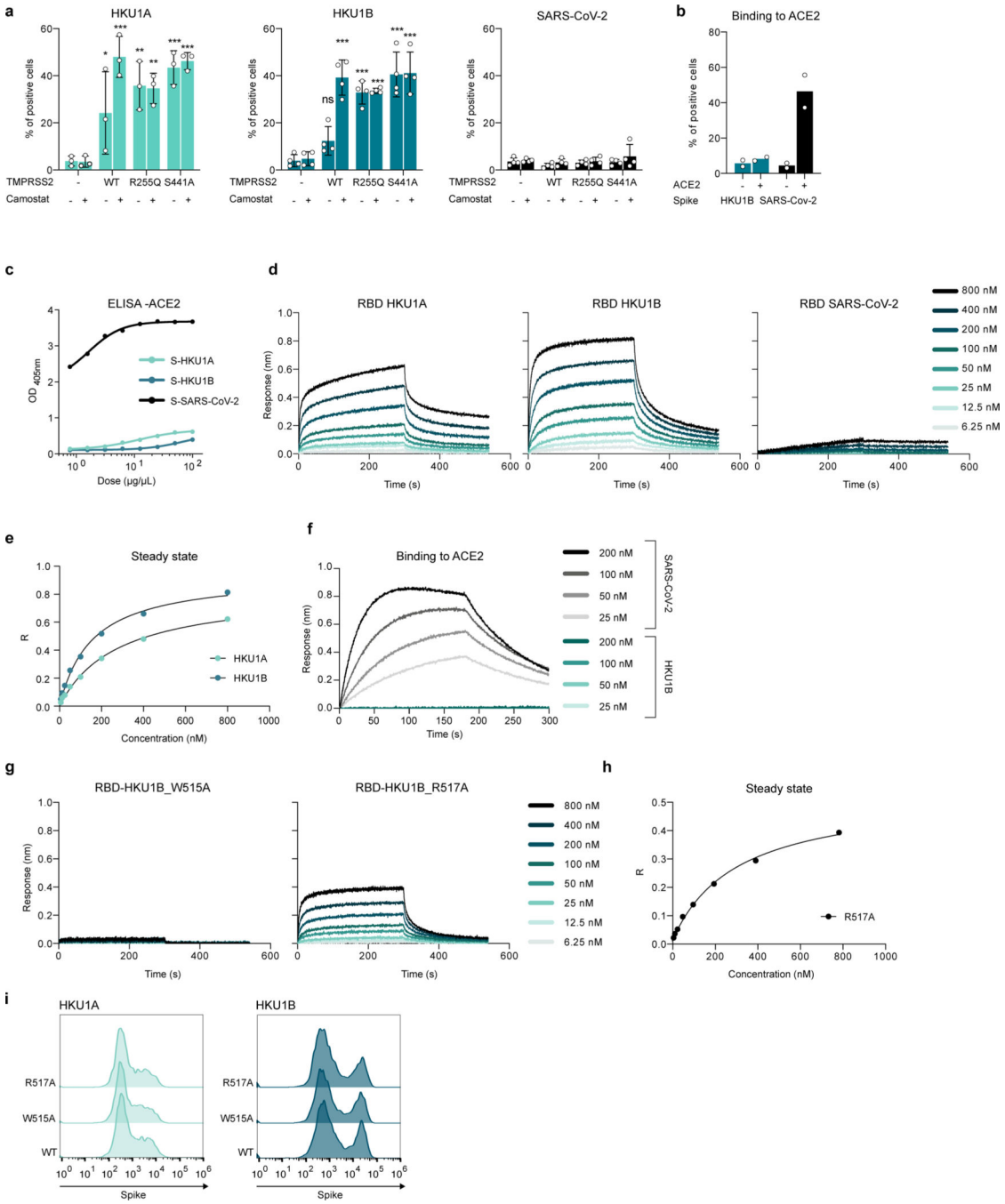


**Extended Data Figure 6. Binding of HKU and SARS-CoV-2 spikes to TMPRSS2 or ACE2. a. Binding of the indicated recombinant spikes to 293T cells expressing TMPRSS2.**

Cells were transfected with WT or mutant TMPRSS2 and incubated or not overnight with 10 µM of Camostat. The spikes were then incubated for 0.5 h and their binding was revealed with streptavidin-647 and measured by flow cytometry. The % of cells binding to TMPRSS2 was quantified. Data are mean ± SD of 3 (HKU1A) or 4 (HKU1B, SARS-CoV-2) independent experiments. Two Way ANOVA with Dunnett's multiple comparisons compared to control cells with or without Camostat. Exact p-values: HKU1A: TMPRSS2 WT-: *0.029, TMPRSS2 WT+:***<0.0001, TMPRSS2 R255Q-: **0.0010, TMPRSS2

R255Q+: **0,0013, TMPRSS2 S441A-: ***0,0001, TMPRSS2 S441A+: ***<0.0001. HKU1B: ***<0.0001. **b. Binding of the indicated recombinant spikes to 293T cells expressing ACE2.** Cells were transfected with ACE2. The spikes were then incubated for 0.5 h and their binding was revealed with streptavidin-647 and measured by flow cytometry. The % of cells binding to ACE2 was quantified. Data are mean of 2 independent experiments. **c. Binding of the indicated soluble spikes on immobilized ACE2 measured by ELISA. d. Binding of S441A TMPRSS2 to HKU1A, HKU1B or SARS-CoV-2 RBD measured by BLI.** The response was measured at the indicated concentrations of spikes. Left: HKU1A. Middle: HKU1B. Right: SARS-CoV-2. One representative experiment of 4 is shown. **e. Determination of the affinity of HKU1A and B RBD for TMPRSS2 using the steady state method.** Circles: Experimental values. Black: Fitting of the experimental data **f. Binding of ACE2 to SARS-CoV-2 or HKU1B RBD quantified by BLI,** at different concentrations of spikes. **g. Binding of S441A TMPRSS2 to HKU1B mutants.** Response was measured by BLI at different concentrations of spikes. Left: HKU1B RBD mutant W515A. B: HKU1B RBD mutant R517A. **h. Determination of the affinity of HKU1B-R517A RBD for TMPRSS2 using the steady state method.** Circles: Experimental values. Black: Fitting of the experimental data. **i. Cell surface levels of WT and mutant HKU1 spikes.** 293T were transfected with the indicated WT or mutant HKU1A or B spikes, expression was measured by flow cytometry after 24 h, using the anti-spike mAb10.

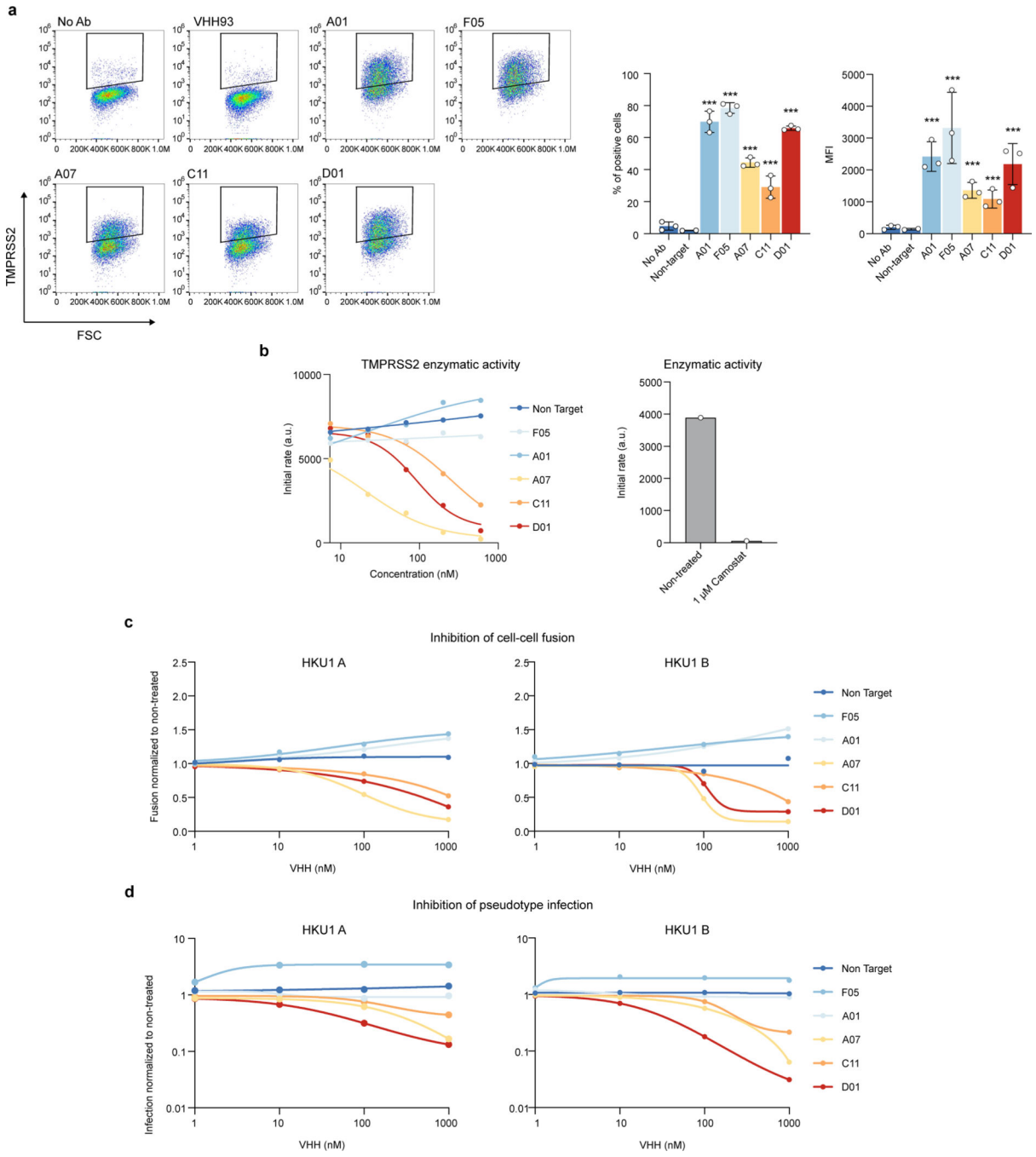


**Extended Data figure 7. Characterization of anti-TMPRSS2 VHHs. a. Binding of VHHs on TMPRSS2-expressing cells.**

293T cells were transfected with TMPRSS2 S441A. Binding of the indicated VHHs (0.5 μM) was assessed by flow cytometry. Left: representative dot plots. Right: Quantification of the percentage of positive cells and MFI (Median Fluorescent Intensity of positive cells). Data are mean ± SD of three independent experiments **b. Effect of VHHs or Camostat on TMPRSS2 enzymatic activity.** Recombinant soluble TMPRSS2 was incubated with the indicated VHHs at different concentrations or with Camostat (1 μM). The initial rate

of enzymatic activity, measured with a fluorescent substrate is plotted. One representative experiment of 3 is shown. **c. Effect of VHHs on HKU1A or HKU1B cell-cell fusion.** 293T GFP-Split cells were cotransfected with TMPRSS2 and HKU1 spike in the presence of indicated amounts of VHH. Fusion was quantified by measuring the GFP area after 20 h. Data were normalized to the non-treated condition for each spike. **d. Effect of VHHs on HKU1A or HKU1B pseudovirus infection**. 293T cells transfected with S441A TMPRSS2 were incubated with the indicated amounts of VHH for 2 h and infected by Luc-encoding pseudovirus. Luminescence was read 48 h post infection. Data were normalized to the non-treated condition for each virus. Data are from one experiment representative of 3. **Statistical analysis**: c: One Way ANOVA with Dunnett's multiple comparisons compared to cells stained with a non-target antibody (VHH93). d: One Way ANOVA on log-transformed data with Dunnett's multiple comparisons compared to cells stained with a non-target antibody (VHH93).

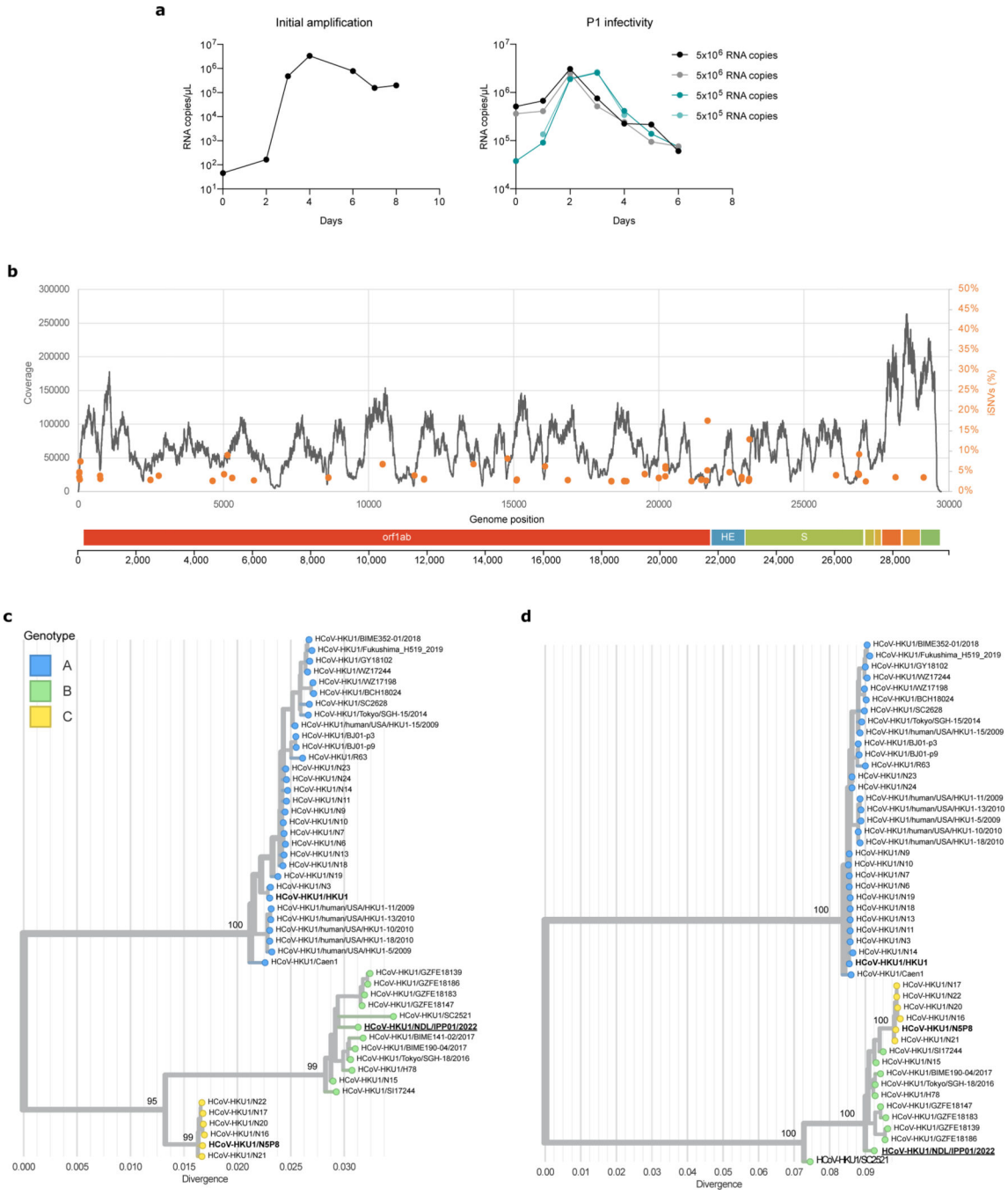


**Extended data Figure 8. Isolation and characterization of a live HKU1B virus.**

**a. Viral RNA copies in the supernatant of HBE cells were quantified by RT-qPCR.** The values at day 0 are the content of the input. Left: initial amplification (first passage). Right: Second amplification of the first passage virus (harvested at day 4) used at two dilutions (1/10 and 1/100) in duplicates. **b. Reads coverage and frequency of minor variants frequencies of the isolate sequencing data (first passage virus).** Intra-sample single-nucleotide variants frequencies were estimated using iVAR[69]. The genome organization of HKU1 is shown below the plot. **c, d. Phylogenetic analysis of HKU1**. Maximum likelihood

phylogenies of human coronavirus HKU1 (n = 48) estimated using IQ-TREE v2 with 1000 replicates from **c**. the complete genome and **d.** spike coding sequences. The tree is midpoint rooted and ultrafast bootstraps values are shown on the main branches. A similar topology was obtained when rooting the tree using another embecovirus (OC43). The tip name corresponding to the newly isolated virus sequence is highlighted in bold and underlined. The tips names corresponding to the recombinant spikes used in this study are shown in bold.

**Extended data Table 1.**

Affinity of the nanobodies for TMPRSS2 S441A and summary of their effect.

| Nanobody | $k_{on}$ (1/Ms) | $k_{off}$ (1/s) | $K_d$ (nM) | Enzymatic activity inhibition | Cell-cell fusion inhibition | Pseudotype infection inhibition |
|---|---|---|---|---|---|---|
| VHH-A01 | $6.4.10^4$ | $5.1.10^{-5}$ | 0.78 | - | - | - |
| VHH-F05 | $7.6.10^4$ | $1.9.10^{-4}$ | 2.6 | - | - | - |
| VHH-A07 | $8.6.10^4$ | $1.1.10^{-3}$ | 13.3 | ++ | ++ | ++ |
| VHH-C11 | $7.0.10^4$ | $2.3.10^{-4}$ | 32.5 | + | + | + |
| VHH-D01 | $7.9.10^4$ | $4.8.10^{-4}$ | 6.0 | + | + | ++ |

## Supplementary Material

Refer to Web version on PubMed Central for supplementary material.

## Acknowledgments

We thank Ali Amara, Timothée Bruel and Nicoletta Casartelli for critical reading of the manuscript, members of the Virus and Immunity Unit for discussions and help, Nathalie Aulner, Nassim Mahtal and the UtechS Photonic BioImaging (UPBI) core facility (Institut Pasteur), Pierre Charneau for help in lentiviral pseudotype preparation, Stefan Pöhlmann for the kind gift of plasmids. NS is funded by the Ministère de l'Enseignement supérieur et de la Recherche. OS laboratory is funded by Institut Pasteur, Fondation pour la Recherche Médicale (FRM), ANRS-MIE, the Vaccine Research Institute (ANR-10-LABX-77), HERA European program (DURABLE consortium), Labex IBEID (ANR-10-LABX-62-IBEID), ANR/FRM Flash Covid PROTEO-SARS-CoV-2 and IDISCOVR. ESL lab is funded by the INCEPTION program (Investissements d'Avenir grant ANR-16-CONV-0005), the NIH PICREID program (Award Number U01AI151758), the HERA European program DURABLE (101102733) and the Labex IBEID (ANR-10-LABX-62-IBEID). HM laboratory is funded by the Institut Pasteur, the Milieu Intérieur Program (ANR-10-LABX-69–01), the INSERM, REACTing, and EU (RECOVER) grants. MMR was supported by the Pasteur-Paris University (PPU) International Doctoral Program and by Institut Pasteur Department of Virology "Bourse de Soudure" fellowship. FAR laboratory is funded by the French ANR (Agence Nationale de la Recherche), grants ANR-13-ISV8–0002-01, ANR-10-LABX-62–10 IBEID, Wellcome Trust collaborative grant (UNS22082), as well as by Institut Pasteur and CNRS. Work in UPBI is funded by grant ANR-10-INSB-04–01 and Région Ile-de-France program DIM1-Health. The funders of this study had no role in study design, data collection, analysis and interpretation, or writing of the article.

## Data availability

Raw sequence data (human reads removed) for the HKU1 virus were deposited in the European Nucleotide Archive (ENA) portal (https://www.ebi.ac.uk/ena/) under bioproject accession number PRJEB64017. The raw data of the main figures are available within the supplementary information. The raw data of the extended data are available from the corresponding author upon reasonable request.

## References


1. Park S, Lee Y, Michelow IC & Choe YJ Global Seasonality of Human Coronaviruses: A Systematic Review. Open Forum Infectious Diseases 7 (2020). 10.1093/ofid/ofaa443
2. Bertram S. et al. TMPRSS2 Activates the Human Coronavirus 229E for Cathepsin-Independent Host Cell Entry and Is Expressed in Viral Target Cells in the Respiratory Epithelium. J. Virol. 87, 6150–6160 (2013). 10.1128/jvi.03372-12 [PubMed: 23536651]
3. Glowacka I. et al. Evidence that TMPRSS2 Activates the Severe Acute Respiratory Syndrome Coronavirus Spike Protein for Membrane Fusion and Reduces Viral Control by the Humoral Immune Response. J. Virol. 85, 4122–4134 (2011). 10.1128/jvi.02232-10 [PubMed: 21325420]
4. Shirato K, Kawase M. & Matsuyama S. Wild-type human coronaviruses prefer cell-surface TMPRSS2 to endosomal cathepsins for cell entry. Virology 517, 9–15 (2018). 10.1016/j.virol.2017.11.012 [PubMed: 29217279]
5. Shirato K, Kawase M. & Matsuyama S. Middle East respiratory syndrome coronavirus infection mediated by the transmembrane serine protease TMPRSS2. J. Virol. 87, 12552–12561 (2013). 10.1128/JVI.01890-13 [PubMed: 24027332]
6. Milewska A. et al. Human coronavirus NL63 utilizes heparan sulfate proteoglycans for attachment to target cells. J. Virol. 88, 13221–13230 (2014). 10.1128/JVI.02078-14 [PubMed: 25187545]
7. Millet JK & Whittaker GR Host cell entry of Middle East respiratory syndrome coronavirus after two-step, furin-mediated activation of the spike protein. Proc. Natl. Acad. Sci. U.S.A. 111, 15214–15219 (2014). 10.1073/pnas.1407087111 [PubMed: 25288733]
8. Shang J. et al. Cell entry mechanisms of SARS-CoV-2. Proc. Natl. Acad. Sci. U.S.A. 117, 11727–11734 (2020). 10.1073/pnas.2003138117 [PubMed: 32376634]
9. Shulla A. et al. A Transmembrane Serine Protease Is Linked to the Severe Acute Respiratory Syndrome Coronavirus Receptor and Activates Virus Entry. J. Virol. 85, 873–882 (2011). 10.1128/JVI.02062-10 [PubMed: 21068237]
10. Hofmann H. et al. Human coronavirus NL63 employs the severe acute respiratory syndrome coronavirus receptor for cellular entry. Proc. Natl. Acad. Sci. U.S.A. 102, 7988–7993 (2005). 10.1073/pnas.0409465102 [PubMed: 15897467]
11. Yeager Curtis L., A. A. R,Wlliams Richard K., B. C. C. & Shapirot Linda H., T. L. A, Holmes Kathryn V.. Human aminopeptidase N is a receptor for human coronavirus 229E. Nature (1992).
12. Hulswit RJG et al. Human coronaviruses OC43 and HKU1 bind to 9-O-acetylated sialic acids via a conserved receptor-binding site in spike protein domain A. Proc. Natl. Acad. Sci. U.S.A. 116, 2681–2690 (2019). 10.1073/pnas.1809667116 [PubMed: 30679277]
13. Woo PCY et al. Characterization and Complete Genome Sequence of a Novel Coronavirus, Coronavirus HKU1, from Patients with Pneumonia. J. Virol. 79, 884–895 (2005). 10.1128/JVI.79.2.884-895.2005 [PubMed: 15613317]
14. Kahn JS & McIntosh K. History and recent advances in coronavirus discovery. Pediatr. Infect. Dis. J. 24, S223–227, discussion S226 (2005). 10.1097/01.inf.0000188166.17324.60 [PubMed: 16378050]
15. Sayama Y. et al. Seroprevalence of four endemic human coronaviruses and, reactivity and neutralization capability against SARS-CoV-2 among children in the Philippines. Sci Rep 13, 2310 (2023). 10.1038/s41598-023-29072-3 [PubMed: 36759702]
16. Killerby ME et al. Human coronavirus circulation in the United States 2014–2017. J. Clin. Virol. 101, 52–56 (2018). 10.1016/j.jcv.2018.01.019 [PubMed: 29427907]
17. Woudenberg T. et al. Humoral immunity to SARS-CoV-2 and seasonal coronaviruses in children and adults in north-eastern France. EBioMedicine 70, 103495 (2021). 10.1016/j.ebiom.2021.103495 [PubMed: 34304047]
18. Ou X. et al. Crystal structure of the receptor binding domain of the spike glycoprotein of human betacoronavirus HKU1. Nat Commun 8, 15216 (2017). 10.1038/ncomms15216 [PubMed: 28534504]
19. Kirchdoerfer RN et al. Pre-fusion structure of a human coronavirus spike protein. Nature 531, 118–121 (2016). 10.1038/nature17200 [PubMed: 26935699]

20. Bestle D. et al. TMPRSS2 and furin are both essential for proteolytic activation of SARS-CoV-2 in human airway cells. Life Science Alliance 3, e202000786 (2020). 10.26508/lsa.202000786
21. Huang X. et al. Human Coronavirus HKU1 Spike Protein Uses O-Acetylated Sialic Acid as an Attachment Receptor Determinant and Employs Hemagglutinin-Esterase Protein as a Receptor-Destroying Enzyme. J. Virol. 89, 7202–7213 (2015). 10.1128/JVI.00854-15 [PubMed: 25926653]
22. Li Z. et al. Synthetic O-acetylated sialosides facilitate functional receptor identification for human respiratory viruses. Nat Chem 13, 496–503 (2021). 10.1038/s41557-021-00655-9 [PubMed: 33753916]
23. Millet JK, Jaimes JA & Whittaker GR Molecular diversity of coronavirus host cell entry receptors. FEMS Microbiol. Rev. 45 (2020). 10.1093/femsre/fuaa057
24. Bugge TH, Antalis TM & Wu Q. Type II transmembrane serine proteases. J. Biol. Chem. 284, 23177–23181 (2009). 10.1074/jbc.R109.021006 [PubMed: 19487698]
25. Fraser BJ et al. Structure and activity of human TMPRSS2 protease implicated in SARS-CoV-2 activation. Nat. Chem. Biol. 18, 963–971 (2022). 10.1038/s41589-022-01059-7 [PubMed: 35676539]
26. Böttcher-Friebertshäuser E. Membrane-Anchored Serine Proteases: Host Cell Factors in Proteolytic Activation of Viral Glycoproteins. Activation of Viruses by Host Proteases, 153–203 (2018). 10.1007/978-3-319-75474-1_8
27. Fraser BJ et al. Structure and activity of human TMPRSS2 protease implicated in SARS-CoV-2 activation. Nat. Chem. Biol. 18, 963–971 (2022). 10.1038/s41589-022-01059-7 [PubMed: 35676539]
28. Lukassen S. et al. SARS-CoV-2 receptor ACE2 and TMPRSS2 are primarily expressed in bronchial transient secretory cells. The EMBO Journal 39, e105114 (2020). 10.15252/embj.20105114 [PubMed: 32246845]
29. Pyrc K. et al. Culturing the Unculturable: Human Coronavirus HKU1 Infects, Replicates, and Produces Progeny Virions in Human Ciliated Airway Epithelial Cell Cultures. J. Virol. 84, 11255–11263 (2010). 10.1128/JVI.00947-10 [PubMed: 20719951]
30. Planchais C. et al. Potent human broadly SARS-CoV-2–neutralizing IgA and IgG antibodies effective against Omicron BA.1 and BA.2. J. Exp. Med. 219 (2022). 10.1084/jem.20220638
31. Buchrieser J. et al. Syncytia formation by SARS-CoV-2-infected cells. EMBO J. 39, e106267 (2020). 10.15252/embj.2020106267 [PubMed: 33051876]
32. Zang R. et al. TMPRSS2 and TMPRSS4 promote SARS-CoV-2 infection of human small intestinal enterocytes. Sci Immunol 5 (2020). 10.1126/sciimmunol.abc3582
33. Kishimoto M. et al. TMPRSS11D and TMPRSS13 Activate the SARS-CoV-2 Spike Protein. Viruses 13 (2021). 10.3390/v13030384
34. Hoffmann M. et al. Camostat mesylate inhibits SARS-CoV-2 activation by TMPRSS2-related proteases and its metabolite GBPA exerts antiviral activity. EBioMedicine 65, 103255 (2021). 10.1016/j.ebiom.2021.103255 [PubMed: 33676899]
35. Koch J. et al. TMPRSS2 expression dictates the entry route used by SARS-CoV-2 to infect host cells. The EMBO Journal 40, e107821 (2021). 10.15252/embj.2021107821 [PubMed: 34159616]
36. Afar Daniel E. H. et al. Catalytic Cleavage of the Androgen-regulated TMPRSS2 Protease Results in Its Secretion by Prostate and Prostate Cancer Epithelia. Cancer Res. 31, 1686–1692 (2001).
37. Hoffmann M. et al. SARS-CoV-2 Cell Entry Depends on ACE2 and TMPRSS2 and Is Blocked by a Clinically Proven Protease Inhibitor. Cell 181, 271–280.e278 (2020). 10.1016/j.cell.2020.02.052 [PubMed: 32142651]
38. Planas D. et al. Resistance of Omicron subvariants BA.2.75.2, BA.4.6, and BQ.1.1 to neutralizing antibodies. Nature Communications 14, 824 (2023). 10.1038/s41467-023-36561-6
39. Dominguez SR et al. Isolation, propagation, genome analysis and epidemiology of HKU1 betacoronaviruses. J. Gen. Virol. 95, 836–848 (2014). 10.1099/vir.0.059832-0 [PubMed: 24394697]
40. Dijkman R. et al. Isolation and Characterization of Current Human Coronavirus Strains in Primary Human Epithelial Cell Cultures Reveal Differences in Target Cell Tropism. J. Virol. 87, 6081–6090 (2013). 10.1128/JVI.03368-12 [PubMed: 23427150]

41. Milewska A. et al. Kallikrein 13 serves as a priming protease during infection by the human coronavirus HKU1. Science Signaling 13, eaba9902 (2020). 10.1126/scisignal.aba9902
42. Koistinen H. et al. The roles of proteases in prostate cancer. IUBMB Life 10.1002/iub.2700
43. Shrimp JH et al. An Enzymatic TMPRSS2 Assay for Assessment of Clinical Candidates and Discovery of Inhibitors as Potential Treatment of COVID-19. ACS Pharmacology & Translational Science 3, 997–1007 (2020). 10.1021/acsptsci.0c00106 [PubMed: 33062952]
44. Suzuki R. et al. Attenuated fusogenicity and pathogenicity of SARS-CoV-2 Omicron variant. Nature 603, 700–705 (2022). 10.1038/s41586-022-04462-1 [PubMed: 35104835]
45. Li W. et al. Angiotensin-converting enzyme 2 is a functional receptor for the SARS coronavirus. Nature 426, 450–454 (2003). 10.1038/nature02145 [PubMed: 14647384]
46. Starr TN et al. ACE2 binding is an ancestral and evolvable trait of sarbecoviruses. Nature 603, 913–918 (2022). 10.1038/s41586-022-04464-z [PubMed: 35114688]

## Additional references

47. Kodaka M. et al. A new cell-based assay to evaluate myogenesis in mouse myoblast C2C12 cells. Exp. Cell Res. 336, 171–181 (2015). 10.1016/j.yexcr.2015.06.015 [PubMed: 26116467]
48. Edie S. et al. Survey of Human Chromosome 21 Gene Expression Effects on Early Development in Danio rerio. G3: Genes, Genomes, Genetics 8, 2215–2223 (2018). 10.1534/g3.118.200144
49. Hayer A. et al. Engulfed cadherin fingers are polarized junctional structures between collectively migrating endothelial cells. Nat. Cell Biol. 18, 1311–1323 (2016). 10.1038/ncb3438 [PubMed: 27842057]
50. Rajah MM et al. SARS-CoV-2 Alpha, Beta, and Delta variants display enhanced Spike-mediated syncytia formation. The EMBO Journal n/a, e108944 (2021). 10.15252/embj.2021108944
51. Iglesias MC et al. Lentiviral vectors encoding HIV-1 polyepitopes induce broad CTL responses in vivo. Mol. Ther. 15, 1203–1210 (2007). 10.1038/sj.mt.6300135 [PubMed: 17375069]
52. Loens K. et al. Performance of Different Mono- and Multiplex Nucleic Acid Amplification Tests on a Multipathogen External Quality Assessment Panel. J. Clin. Microbiol. 50, 977–987 (2012). 10.1128/jcm.00200-11 [PubMed: 22170925]
53. Matranga CB et al. Enhanced methods for unbiased deep sequencing of Lassa and Ebola RNA viruses from clinical and biological samples. Genome Biol 15, 519 (2014). 10.1186/preaccept-1698056557139770 [PubMed: 25403361]
54. Bolger AM, Lohse M. & Usadel B. Trimmomatic: a flexible trimmer for Illumina sequence data. Bioinformatics 30, 2114–2120 (2014). 10.1093/bioinformatics/btu170 [PubMed: 24695404]
55. Li D. et al. MEGAHIT v1.0: A fast and scalable metagenome assembler driven by advanced methodologies and community practices. Methods 102, 3–11 (2016). 10.1016/j.ymeth.2016.02.020 [PubMed: 27012178]
56. Buchfink B, Xie C. & Huson DH Fast and sensitive protein alignment using DIAMOND. Nat. Methods 12, 59–60 (2015). 10.1038/nmeth.3176 [PubMed: 25402007]
57. Katoh K. & Standley DM MAFFT Multiple Sequence Alignment Software Version 7: Improvements in Performance and Usability. Mol. Biol. Evol. 30, 772–780 (2013). 10.1093/molbev/mst010 [PubMed: 23329690]
58. Martin DP, Murrell B, Khoosal A. & Muhire B. in Bioinformatics: Volume I: Data, Sequence Analysis, and Evolution (ed Keith Jonathan M.) 433–460 (Springer New York, 2017).
59. Kalyaanamoorthy S, Minh BQ, Wong TKF, von Haeseler A. & Jermiin LS ModelFinder: fast model selection for accurate phylogenetic estimates. Nat. Methods 14, 587–589 (2017). 10.1038/nmeth.4285 [PubMed: 28481363]
60. Hoang DT, Chernomor O, von Haeseler A, Minh BQ & Vinh LS UFBoot2: Improving the Ultrafast Bootstrap Approximation. Mol. Biol. Evol. 35, 518–522 (2017). 10.1093/molbev/msx281
61. Hadfield J. et al. Nextstrain: real-time tracking of pathogen evolution. Bioinformatics 34, 4121–4123 (2018). 10.1093/bioinformatics/bty407 [PubMed: 29790939]

62. Gransagne M. et al. Development of a highly specific and sensitive VHH-based sandwich immunoassay for the detection of the SARS-CoV-2 nucleoprotein. J. Biol. Chem. 298, 101290 (2022). 10.1016/j.jbc.2021.101290 [PubMed: 34678315]

63. Robinot R. et al. SARS-CoV-2 infection induces the dedifferentiation of multiciliated cells and impairs mucociliary clearance. Nature Communications 12, 4354 (2021). 10.1038/s41467-021-24521-x

64. Hsieh C-L et al. Structure-based design of prefusion-stabilized SARS-CoV-2 spikes. Science 369, 1501–1505 (2020). 10.1126/science.abd0826 [PubMed: 32703906]

65. Lorin V. & Mouquet H. Efficient generation of human IgA monoclonal antibodies. J. Immunol. Methods 422, 102–110 (2015). 10.1016/j.jim.2015.04.010 [PubMed: 25910833]

66. Mouquet H. et al. Memory B cell antibodies to HIV-1 gp140 cloned from individuals infected with clade A and B viruses. PLoS One 6, e24078 (2011). 10.1371/journal.pone.0024078 [PubMed: 21931643]

67. Lafaye P, Achour I, England P, Duyckaerts C. & Rougeon F. Single-domain antibodies recognize selectively small oligomeric forms of amyloid beta, prevent Abeta-induced neurotoxicity and inhibit fibril formation. Mol. Immunol. 46, 695–704 (2009). 10.1016/j.molimm.2008.09.008 [PubMed: 18930548]

68. Li Q. et al. Generation of nanobodies acting as silent and positive allosteric modulators of the α7 nicotinic acetylcholine receptor. Cell. Mol. Life Sci. 80, 164 (2023). 10.1007/s00018-023-04779-8 [PubMed: 37231269]

69. Grubaugh ND et al. An amplicon-based sequencing framework for accurately measuring intrahost virus diversity using PrimalSeq and iVar. Genome Biology 20, 8 (2019). 10.1186/s13059-018-1618-7 [PubMed: 30621750]

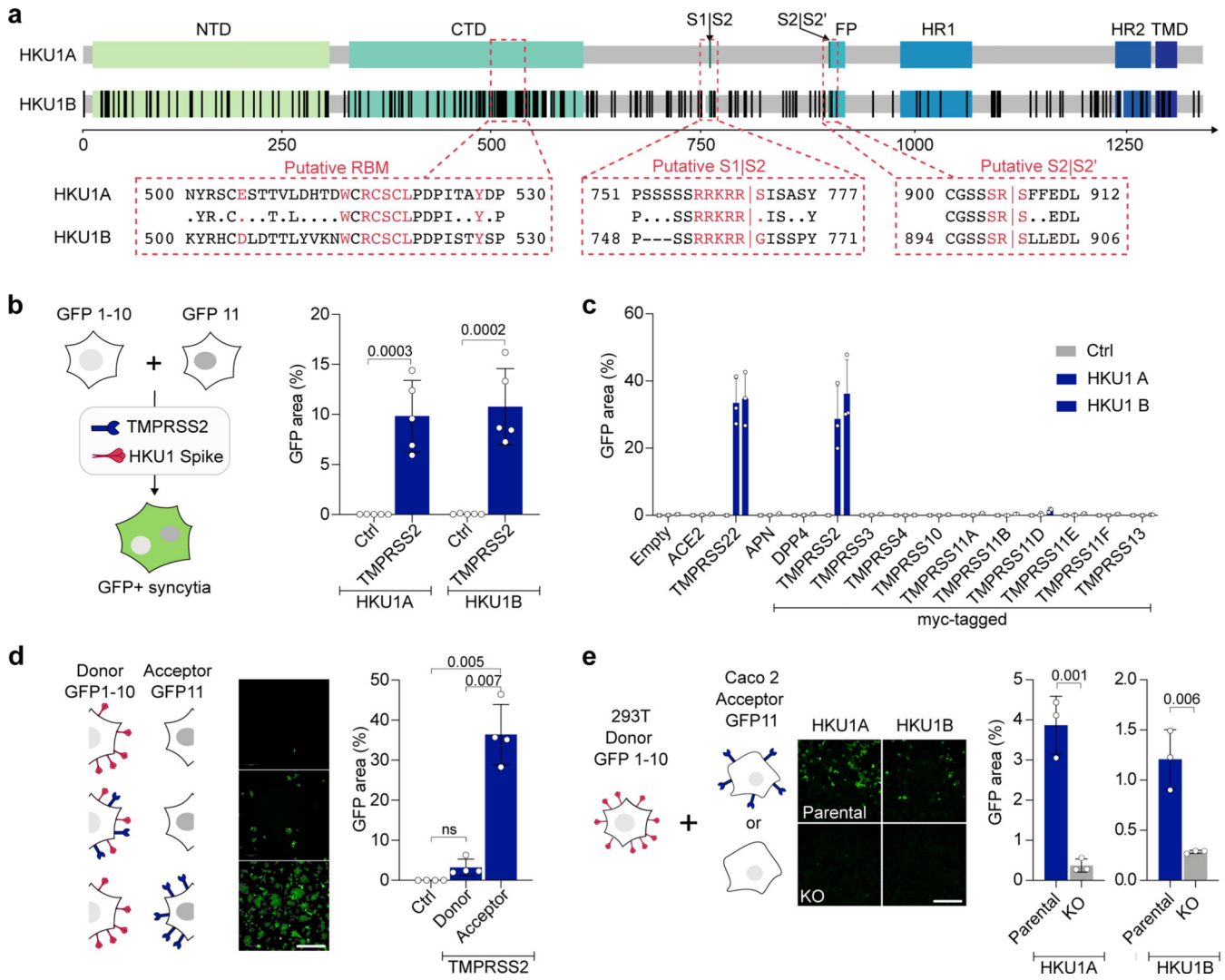


**Figure 1. TMPRSS2 triggers HKU1 spike fusion.**

**a. Alignment of HKU1A and B spikes**. TD: N-terminal Domain. CTD: C-terminal domain. FP: Fusion-peptide. HR11/2: Heptad-Repeat 1/2. TMD: Transmembrane Domain. Black: mismatch, white: deletion, boxed text (Red): amino-acids of the putative RBM, S1/S2 and S2/S2' cleavage site. **b. TMPRSS2 mediates HKU1 cell-cell fusion.** 293T cells expressing either GFP1–10 or GFP-11 (293T-GFP-split cells) were transfected with HKU1 spike and TMPRSS2 or pQCXIP-empty control (Ctrl) plasmids, fusion was quantified by measuring the GFP area after 20 h. Data are mean ± SD of 5 independent experiments. **c. Effect of a panel of proteases on cell-cell fusion.** 293T-GFP-split cells were transfected with HKU1 spike and the indicated protease plasmids, fusion was quantified by measuring the GFP area after 48 h. Data are mean ± SD of 3 independent experiments. **d. TMPRSS2 has to be on the acceptor cell.** TMPRSS2 was transfected either in donor cells and HKU1A spike or in acceptor cells. Fusion was quantified after 20 h. Left: experimental design. Middle: representative images of GFP+ cells. Right: fusion quantification. bar: 400 μm. Data are mean ± SD of 4 independent experiments. **e. Role of endogenous TMPRSS2.** 293T donor cells expressing HKU1A spike were mixed with Caco2 acceptor cells knocked-out or not for

the *tmprss2* gene. Left: experimental design. Middle: representative images of GFP+ cells. Right: fusion was quantified by measuring the GFP area after 20 h of coculture. Data are mean ± SD of 3 independent experiments. **Statistical analysis:** b, d, e: Two-sided unpaired t-test compared to control/parental condition. c: one Way ANOVA on non-normalized data with Tukey's multiple comparisons.

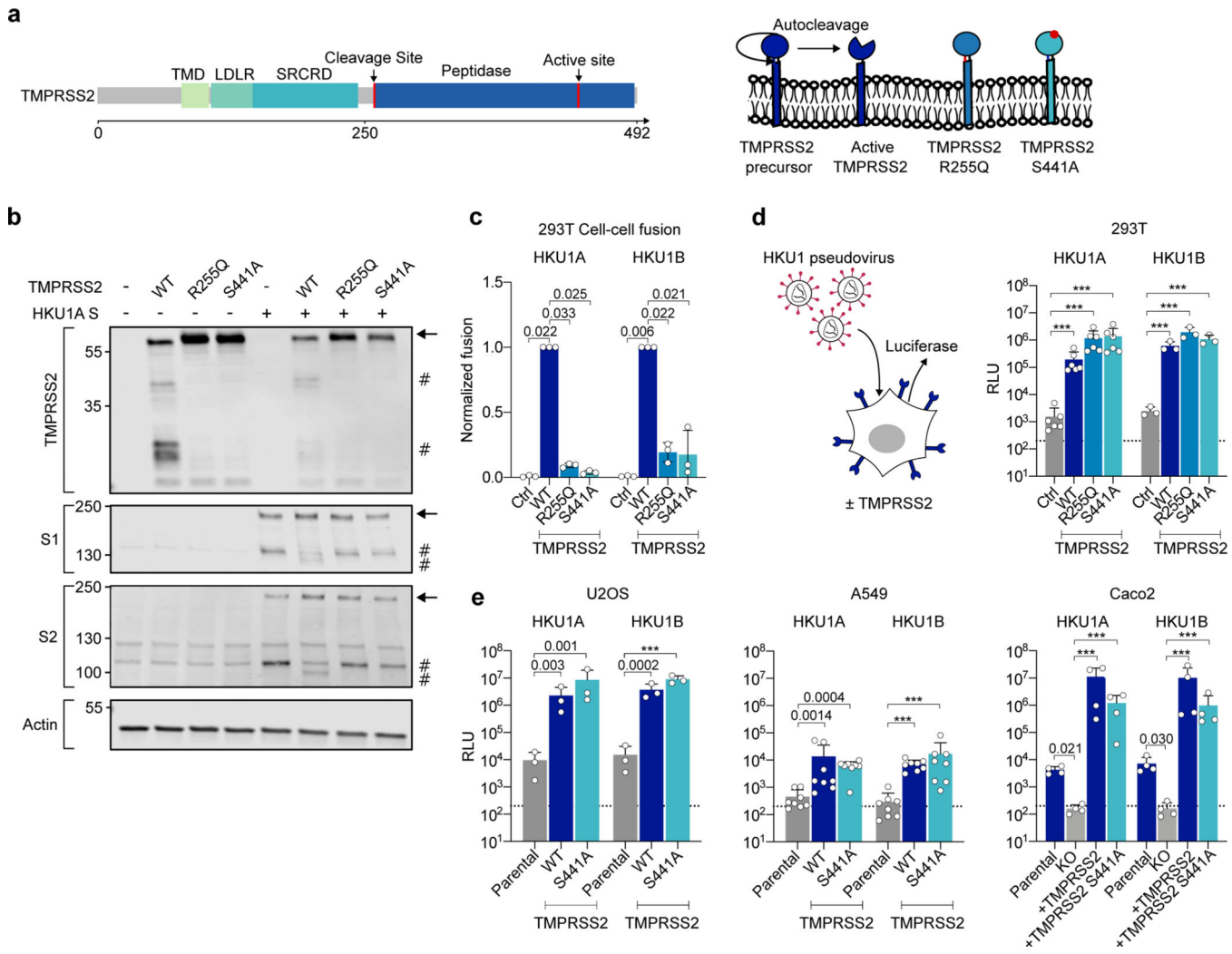


**Figure 2. Effect of wild-type and mutant TMPRSS2 on HKU1 cell-cell fusion and pseudovirus infection.**

**a. TMPRSS2 protein.** TMPRSS2 is composed of a Transmembrane Domain (TMD), a class A LDL receptor domain (LDLR), a Scavenger Receptor Cysteine-2 rich domain (SRCRD) and a serine peptidase. TMPRSS2 precursor autocleaves at R255-L256, resulting in an active protease. **b. TMPRSS2 and spike cleavage.** WB of 293T transfected with HKU1A spike and indicated TMPRSS2 mutants. One membrane was probed for S1, TMPRSS2 and actin, another for S2 and actin. For gel source data, see SI 1a, b. Representative blots of 3 independent experiments. Molecular weights: kDa. Arrows and # denote the uncleaved and cleaved proteins, respectively. **c. Catalytically inactive TMPRSS2 mutants do not trigger HKU1 cell-cell fusion**. Fusion of 293T-GFP split transfected with HKU1 spike and mutant TMPRSS2 was quantified after 20 h and normalized to WT TMPRSS2. Ctrl: pQCXIP-Empty. Left: HKU1A. Right: HKU1B. Data are mean ± SD of 3 independent experiments. **d. Catalytically inactive TMPRSS2 mutants mediate HKU1 pseudovirus infection.** 293T transfected with WT or mutant TMPRSS2 were infected by Luc-encoding HKU1 pseudovirus. Luminescence was read 48 h post infection. Dotted line indicates background in non-infected cells. Ctrl: pQCXIP-Empty. Data are mean ± SD of 6 (HKU1A)

or 3 (HKU1B) independent experiments. **e. HKU1 pseudovirus infection in cell lines stably expressing TMPRSS2**. Left: U2OS cells. Middle: A549 cells. Right: Caco2 cells. The TMPRSS2 KO Caco2 cells were stably transduced with indicated TMPRSS2. Data are mean ± SD of 3 (U2OS), 8 (A549), 4 (Caco2) independent experiments. **Statistical analysis:** c: one-way ANOVA on non-normalized data with Dunnett's multi-comparison test compared to WT TMPRSS2 expressing cells. d, e: one-way ANOVA on log-transformed data with Dunnett's multi-comparison test compared to the untransfected (d), parental (e: U2OS and A549) or KO cells (e: Caco2), ***$p<0.0001$.

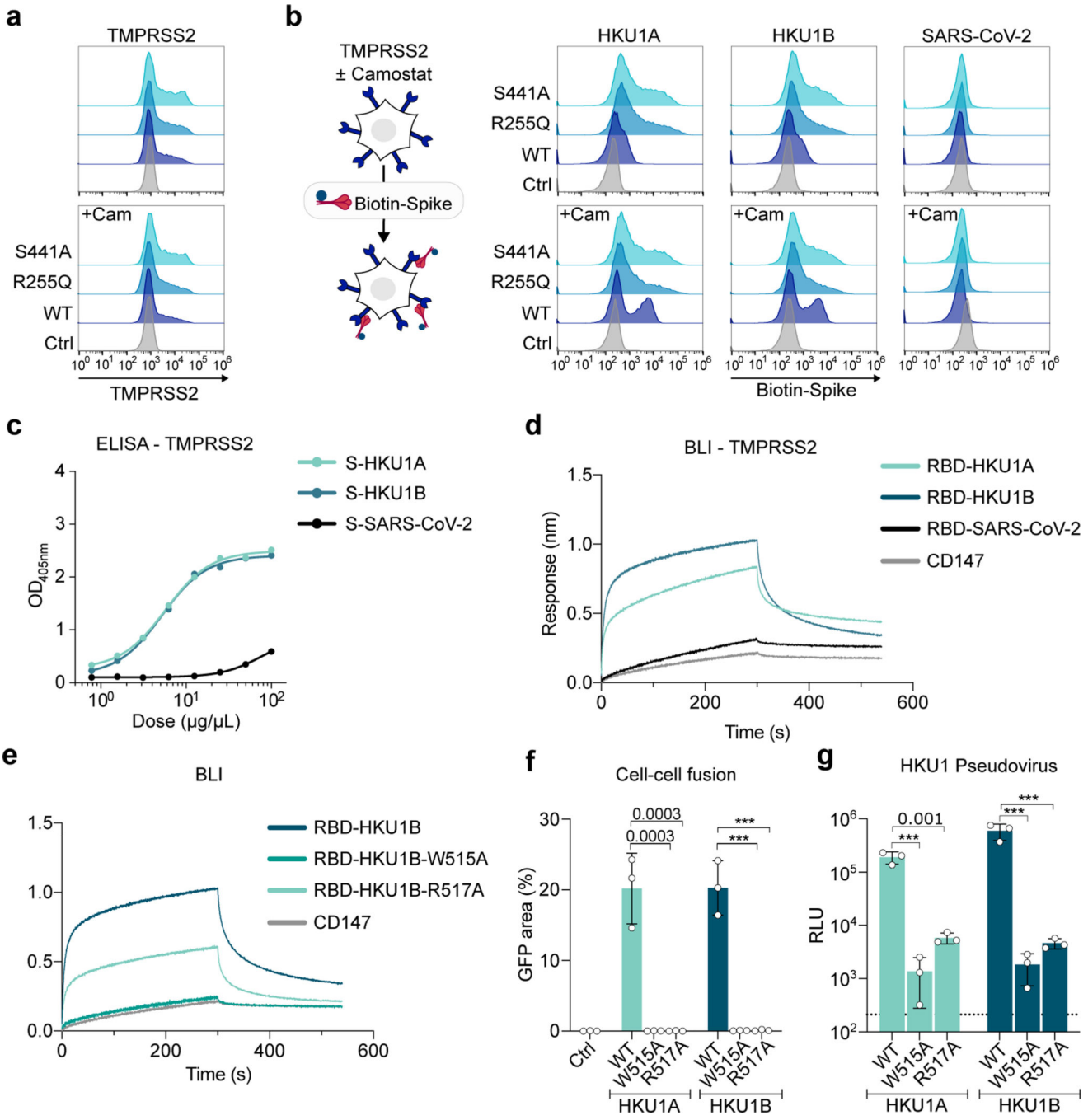


**Figure 3. Analysis of HKU1 spike binding to TMPRSS2.**

**a-b. Binding of soluble HKU1 spikes to 293T cells expressing TMPRSS2.** Cells were transfected with TMPRSS2 mutants and incubated or not with 10 µM of Camostat. **a. TMPRSS2 levels** (assessed with a commercial Ab) **b. Binding of soluble biotinylated trimeric spikes** measured by flow cytometry. One representative experiment of 3 is shown. Ctrl: pQCXIP-Empty control plasmid. **c. Binding of HKU and SARS-CoV-2 spikes on immobilized WT TMPRSS2 measured by ELISA.** Mean of 2 independent experiments. **d. Binding of S441A TMPRSS2 to RBD coated receptors quantified by Bio-layer**

**interferometry (BLI).** One representative experiment of 4 is shown. **e, f, g. Properties of W515A and R517A mutant HKU1 spikes.** Binding of TMPRSS2 to wild type or mutant RBD coated receptors quantified by BLI. One representative experiment of 4 is shown. **f.** 293T GFP-split cells were transfected with TMPRSS2 and the indicated HKU1 mutant spikes, fusion was quantified by measuring the GFP area after 24 h. **g.** 293T cells expressing TMPRSS2 were infected by Luc-encoding mutant HKU1 pseudovirus. Luminescence was read 48 h post infection. Dotted line indicates background. Data are mean ± SD of 3 independent experiments. **Statistical analysis:** f: one-way ANOVA on non-normalized data with Dunnett's multi-comparison test compared to WT TMPRSS2 expressing cells. g: one-way ANOVA on log-transformed data with Dunnett's multi-comparison test compared to WT Spike pseudotypes *$p<0.05$, **$p<0.01$, ***$p<0.001$.

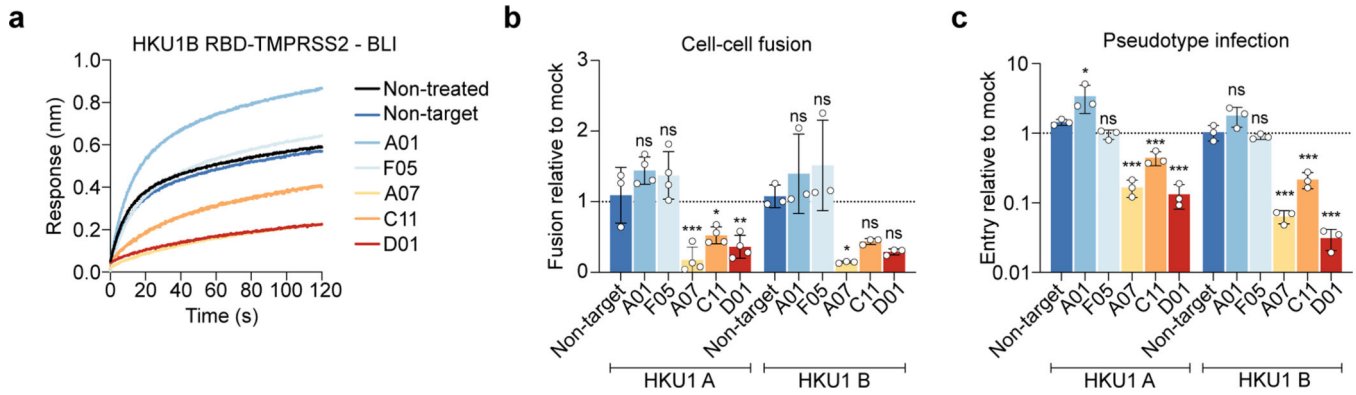


**Figure 4. Anti-TMPRSS2 VHH nanobodies inhibit HKU1 binding to TMPRSS2, cell-cell fusion and pseudovirus infection.**

**a. Effect of VHHs on binding of HKU1B RBD to TMPRSS2 measured by BLI**. One representative experiment of 2 is shown **b. Effect of VHHs on HKU1-mediated cell-cell fusion.** 293T GFP-Split cells were transfected with TMPRSS2 and HKU1 spike in the presence of 1 $\mu$M of VHH, fusion was quantified 20 h later. Data were normalized to the non-VHH treated condition (dotted line). Data are mean ± SD of 4 independent experiments. **c. Effect of VHHs on HKU pseudovirus infection**. 293T cells transfected with S441A TMPRSS2 were treated with 1 $\mu$M VHH 2 h before infection. Luminescence was read 48 h post infection. Data were normalized to the non-treated condition for each virus (dotted line). Data are mean ± SD of 3 independent experiments. **Statistical analysis**: b: one Way ANOVA data with Dunnett's multiple comparisons compared to non-target VHH c: one Way ANOVA on log-transformed data with Dunnett's multiple comparisons compared to non-target VHH *p<0.05, **p<0.01, ***p<0.001. p-values. Fusion, HKU1A: A07 0.0005, C11: 0.025, D01: 0.004, HKU1B: A07: 0.029, Infection: HKU1A: A01: 0.016, A07: <0.0001, C11:0.0009, D01:<0.0001 HKU1B: A07/C11/D01: <0.0001

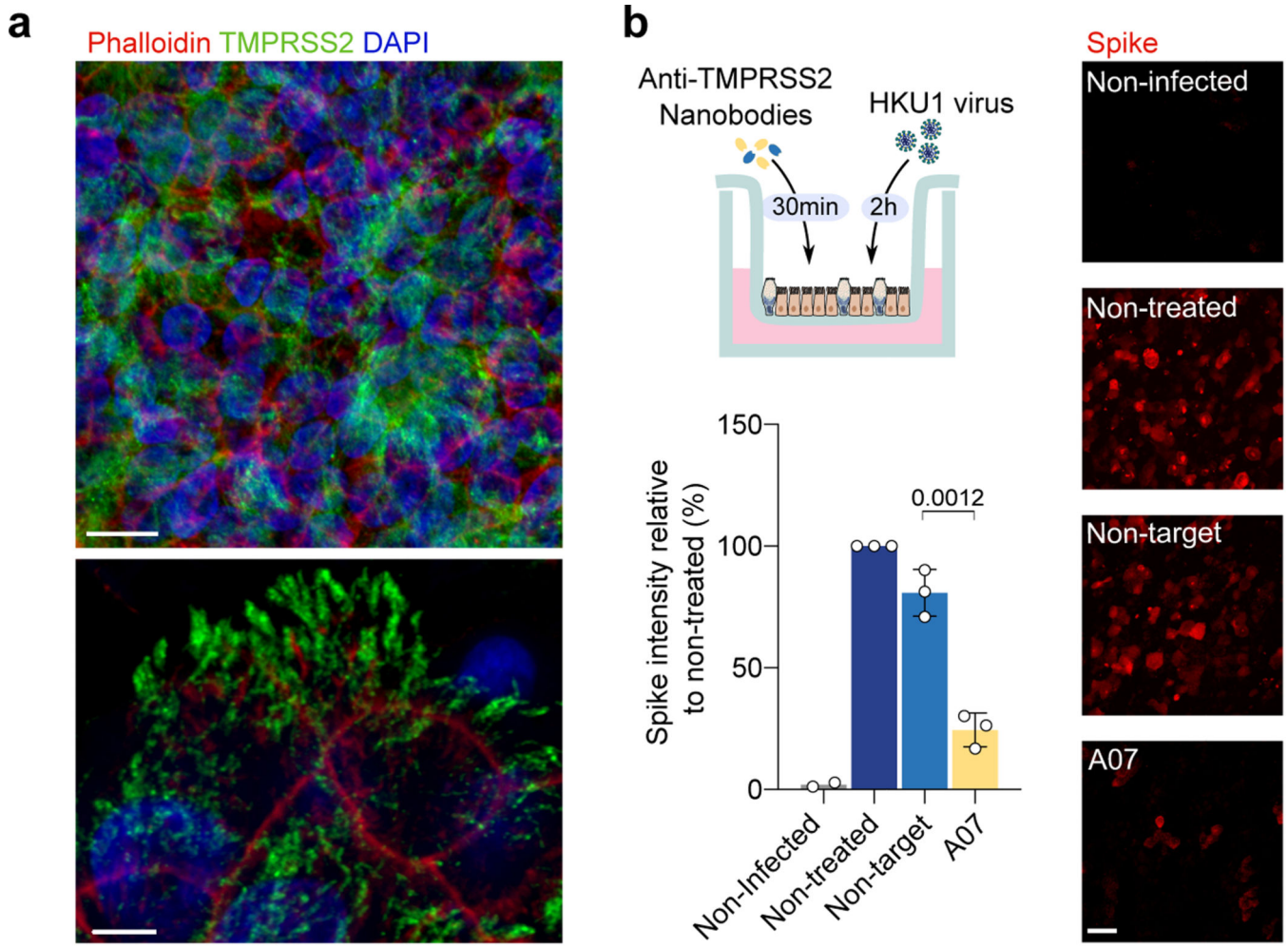


**Figure 5. Live HKU1 virus infection of human bronchial epithelial (HBE) cells.**

**a. TMPRSS2 staining of HBE cells**. Red: Phalloidin, Blue: DAPI, Green: TMPRSS2 stained with VHH A01-Fc. Scale bars: top, 10 μm; bottom, 5 μm. Images are representative of 3 independent experiments. **b. Effect of the anti-TMPRSS2 VHH (A07) on HKU1 infection.** The experimental design is represented. Infected cells were visualized with an anti-spike antibody and scored. Representative images of spike staining 48 h post-infection are shown. Spike pixel intensity in 5 random fields per experiment was measured and normalized to the intensity in the infected but non-treated condition. Data are mean ± SD of 3 independent experiments for infected conditions, and mean of 2 for uninfected condition. Scale bar: 20 μm. **Statistical analysis:** Two-sided unpaired t-test compared to non-target VHH.

**Table 1:**

Affinity ($K_d$) of the indicated RBD for TMPRSS2 or ACE2. ND (Non-Detectable) denotes proteins for which interaction with the loaded sensor was similar or below the interaction with an empty sensor.

| Sensor | Ligand | $K_d$ (nM) |
|---|---|---|
| RBD-HKU1A | TMPRSS2 | 334.3 ± 66.2 |
| RBD-HKU1B | TMPRSS2 | 136.7 ± 20.8 |
| RBD-HKU1B-W515A | TMPRSS2 | ND |
| RBD-HKU1B-R517A | TMPRSS2 | 376.2 ± 96.4 |
| RBD-SARS-CoV-2 | TMPRSS2 | ND |
| RBD-HKU1B | ACE2 | ND |
| RBD-SARS-CoV-2 | ACE2 | 92 |